Biogeosciences Discuss., 12, 3731–3824, 2015
www.biogeosciences-discuss.net/12/3731/2015/
doi:10.5194/bgd-12-3731-2015

Biogeosciences
Discussions
Open Access

Drivers and uncertainties of future global marine primary production in marine ecosystem models

C. Laufkötter[1], M. Vogt[1], N. Gruber[1], M. Aita-Noguchi[7], O. Aumont[2], L. Bopp[3], E. Buitenhuis[4], S. C. Doney[5], J. Dunne[6], T. Hashioka[7], J. Hauck[8], T. Hirata[9], J. John[6], C. Le Quéré[14], I. D. Lima[5], H. Nakano[13], R. Seferian[15], I. Totterdell[10], M. Vichi[11,12], and C. Völker[8]

[1]Environmental Physics, Institute of Biogeochemistry and Pollutant Dynamics, ETH Zürich, Zürich, Switzerland
[2]Laboratoire de Physique des Oceans, Centre IRD de Bretagne, Plouzane, France
[3]Laboratoire des sciences du climat et de l'Environnement (LSCE), IPSL, CEA-UVSQ-CNRS,UMR8212, Gif-sur-Yvette, France
[4]Tyndall Centre for Climate Change Research, School of Environmental Sciences, University of East Anglia, Norwich, UK
[5]Woods Hole Oceanographic Institution, Department of Marine Chemistry & Geochemistry, Woods Hole, MA, USA
[6]NOAA Geophysical Fluid Dynamics Laboratory, Princeton, New Jersey, USA
[7]Core Research for Evolutional Science and Technology, Japan Science and Technology Agency, Tokyo, Japan

[8]Alfred Wegener Institute, Helmholtz Centre for Polar and Marine Research, Bremerhaven, Germany
[9]Faculty of Environmental Earth Science, Hokkaido University, Sapporo, Kita Ward, Japan
[10]Met Office, Exeter, UK
[11]Centro Euro-Mediterraneo sui Cambiamenti Climatici (CMCC), Bologna, Italy
[12]Department of Oceanography, University of Cape Town (UCT), Cape Town, South Africa
[13]Meteorological Research Institute, Tsukuba, Ibaraki, Japan
[14]Tyndall Centre for Climate Change Research, University of East Anglia, Norwich Research Park, Norwich NR47TJ, UK
[15]CNRM-GAME, Centre National de Recherche Météorologique-Groupe d'Etude de l'Atmosphère Météorologique, Météo-France/CNRS, 42 Avenue Gaspard Coriolis, 31100 Toulouse, France

Received: 19 December 2014 – Accepted: 19 January 2015 – Published: 27 February 2015

Correspondence to: C. Laufkötter (charlotte.laufkoetter@env.ethz.ch)

Published by Copernicus Publications on behalf of the European Geosciences Union.

Abstract

Past model studies have projected a global decrease in marine net primary production (NPP) over the 21st century, but these studies focused on the multi-model mean and mostly ignored the large inter-model differences. Here, we analyze model simulated changes of NPP for the 21st century under IPCC's high emission scenario RCP8.5 using a suite of nine coupled carbon–climate Earth System Models with embedded marine ecosystem models with a focus on the spread between the different models and the underlying reasons. Globally, five out of the nine models show a decrease in NPP over the course of the 21st century, while three show no significant trend and one even simulates an increase. The largest model spread occurs in the low latitudes (between 30° S and 30° N), with individual models simulating relative changes between −25 and +40 %. In this region, the inter-quartile range of the differences between the 2012–2031 average and the 2081–2100 average is up to 3 mol C m^{-2} yr^{-1}. These large differences in future change mirror large differences in present day NPP. Of the seven models diagnosing a net decrease in NPP in the low latitudes, only three simulate this to be a consequence of the classical interpretation, i.e., a stronger nutrient limitation due to increased stratification and reduced upwelling. In the other four, warming-induced increases in phytoplankton growth outbalance the stronger nutrient limitation. However, temperature-driven increases in grazing and other loss processes cause a net decrease in phytoplankton biomass and reduces NPP despite higher growth rates. One model projects a strong increase in NPP in the low latitudes, caused by an intensification of the microbial loop, while the remaining model simulates changes of less than 0.5 %. While there is more consistency in the modeled increase in NPP in the Southern Ocean, the regional inter-model range is also very substantial. In most models, this increase in NPP is driven by temperature, but is also modulated by changes in light, macronutrients and iron as well as grazing. Overall, current projections of future changes in global marine NPP are subject to large uncertainties

and necessitate a dedicated and sustained effort to improve the models and the concepts and data that guide their development.

1 Introduction

By producing organic matter through photosynthesis, marine phytoplankton form the base of the marine food web, control the amount of food available for higher trophic levels, and drive the majority of the ocean's biogeochemical cycles, particularly that of carbon. The net formation rate of organic carbon by phytoplankton, i.e., net primary production, NPP, is a key determinant for the export of organic carbon from the surface ocean, thereby governing how ocean biology impacts the ocean/atmosphere balance of CO_2 (Falkowski et al., 2003; Sarmiento and Gruber, 2006). Accurate projections of future patterns of NPP may be crucial not only to estimate the potential impacts of climate change on marine ecosystems and fishery yields, but also to properly assess the evolution of the ocean carbon sink under anthropogenic climate change.

Several authors have analyzed trends in future NPP and the underlying drivers, using models of strongly varying complexity and spatial resolution with regard to both the physical and the ecosystem components and also investigating different climate change scenarios. In the majority of these studies, global marine NPP was projected to decrease in response to future climate change (Bopp et al., 2001, 2013; Boyd and Doney, 2002; Steinacher et al., 2010; Marinov et al., 2013). The main mechanism suggested was a decrease in the upward supply of nutrients in the low latitudes because of increased vertical stratification (Bopp et al., 2001; Steinacher et al., 2010). Lower nutrient availability resulted then in a decrease in phytoplankton growth and therefore reduced NPP.

But a few studies produced contradicting results, i.e., they reported global NPP increases as climate change progresses over the 21st century (Sarmiento et al., 2004; Schmittner et al., 2008). Taucher and Oschlies (2011) analyzed the model of Schmittner et al. (2008), and showed that the increase in NPP is caused by the warmer temperatures enhancing phytoplankton growth, overcoming the suppression owing to stronger nutrient stress. Yet, some models used in Steinacher et al. (2010) have a stronger temperature dependence of the growth rate than that used in the Schmittner et al. (2008) model, but they still project a decrease in NPP.

On a broad-scale regional basis, there is more agreement with regard to the sign of the changes of NPP. Most models agree on a pattern of decreases in NPP in the low latitudes, and an increase in the high latitudes, especially the Arctic and the Southern Ocean. The low latitude decrease tends to dominate the global response, while the high latitude increase results from warmer temperatures, stronger vertical stratification leading to higher average light levels in the surface mixed layer, and higher iron availability (Steinacher et al., 2010; Bopp et al., 2001).

The past century provides very little constraint on the impact of long-term climate change on marine productivity, largely because of the lack of long-term (> 50 years) observations. Using a combination of in situ observations of chlorophyll and of ocean transparency, Boyce et al. (2010) suggested a substantial decrease in phytoplankton biomass over the last 50 years, implying a very strong response of phytoplankton to ocean warming. This result has been met with a lot of scepticism (e.g. Rykaczewski and Dunne, 2011), especially because an independent assessment of long-term trends in ocean color by Wernand et al. (2013) implied no overall global trend. Smaller decreases in NPP (−6 % over 50 years) were suggested by a hindcast model simulation, where a marine ecosystem model was forced with observed atmospheric variability and changes over the last 50 years (Laufkötter et al., 2013). The satellite observations since late 1997 suggest a negative correlation between sea surface temperature and NPP (Behrenfeld et al., 2006), but the observation period is clearly too short to distinguish natural fluctuations from an anthropogenically driven trend in global marine NPP (Henson et al., 2011; Antoine et al., 2005; Gregg, 2003).

Far less work has been done regarding future trends of specific plankton functional types (PFT), despite their importance in shaping ecosystem structure and function (Le Quéré et al., 2005). Experiments have revealed a negative relationship between warmer waters and phytoplankton cell size, suggesting that future warming may tend to favor small phytoplankton (Morán et al., 2010). Moreover, using year-to-year variability associated with the North Atlantic Oscillation and the Southern Annular Mode, Alvain et al. (2013) found that more stagnant conditions and warmer temperatures tend to disfavor diatoms, suggesting that diatoms will become less prevalent in the future. The few modeling studies available support this view, i.e., they reported global decreases in the diatom fraction and a shift towards smaller size classes (Bopp et al., 2005; Marinov et al., 2010, 2013; Dutkiewicz et al., 2013). In these models, this shift was driven by increased nutrient limitation that affected diatoms more strongly than small phytoplankton.

While published studies emphasized the role of changes in bottom-up factors in explaining the changes in NPP, top-down control by zooplankton grazing may also drive future changes in total NPP or phytoplankton composition. This mechanism is intriguing, since top-down control was recently identified as one of the main drivers of phytoplankton competition during blooms in several ecosystem models (Hashioka et al., 2013; Prowe et al., 2011), affecting the onset of the spring bloom (Behrenfeld, 2010; Behrenfeld et al., 2013), influences primary production in a trait-based ecosystem model (Prowe et al., 2012) and has been shown to affect NPP and EP changes on regional scales (Bopp et al., 2001).

Previous efforts in comparing different models with regard to future trends in NPP have analyzed the multi-model mean response and focused on identifying regions of consistent changes and mechanisms among models (Steinacher et al., 2010; Bopp et al., 2013). By largely disregarding the regions of large inconsistencies, this focus may have underestimated the uncertainty associated with current projections of future marine NPP changes. This is well illustrated by the most recent model comparison study by Bopp et al. (2013), where the spread in the global NPP change between the 10 investigated global models for a given climate change scenario was larger (−20 and +2 %) than the NPP difference between the different scenarios for the multi-model mean (−9 to −2 %), demonstrating that the model uncertainty is larger than the scenario uncertainty.

Reasons why models differ are seldom investigated in model comparison studies. In particular, it is often not readily clear whether the large spread in model projections is mainly caused by differences in the underlying ocean circulation model, by differences in the complexity of the ecosystem models or by differences in the parameterizations leading to differing sensitivities to e.g., changes in temperature, nutrients and light. Such information is needed, however, in order to improve the existing models and to develop the next generation marine ecosystem models.

In this work we go beyond the basic analysis of the multi-model mean and the identification of regions of model consistency. Our aim is to identify where models differ and by how much, and then determine why they do so, i.e., identify the underlying drivers of change. To this end, we use results from a set of 8 global marine ecosystem models coupled to or forced with 9 coupled carbon–climate Earth System Models, which have simulated the future evolution of marine NPP under the Intergovernmental Panel on Climate Change (IPCC) Representative Concentration Pathways (RCP) 8.5 (van Vuuren et al., 2011). We decompose the long-term changes in NPP into the contributions of the different phytoplankton functional types and then identify the relative importance and uncertainty of the main drivers. We discuss the diversity of responses caused by the ecosystem parameterizations and compare them to uncertainties in the underlying physical forcing. We demonstrate that (i) current marine ecosystem models are revealing more spread with regard to future changes of NPP than shown previously, and (ii) even where the models simulate consistent changes, the underlying drivers are quite different. In particular, we highlight the critical, but not well quantified role of temperature change in determining the future changes in NPP.

2 Methods

2.1 Model descriptions

We use projections for the 2012–2100 period of 9 model simulations for IPCCs RCP8.5 scenario from either the "MARine Ecosystem Model Intercomparison Project" (MAREMIP, http://pft.ees.hokudai.ac.jp/maremip/index.shtml, Vogt et al., 2013; Sailley et al., 2013; Hashioka et al., 2013) and/or the "Coupled Model Intercomparison Project 5" (CMIP5, Taylor et al., 2012). As we aim to include an analysis of the effect of PFT composition on NPP changes, we included only data from those models that possess at least 2 phytoplankton PFTs and at least one zooplankton PFT. For the models taken from the CMIP5 archive, only the first ensemble member (r1ip1) was used.

These criteria led us to use data from eight different marine ecosystem models: diat-HadOCC, BEC, TOPAZ, PISCES, MEM, PELAGOS, REcoM2 and PlankTOM5.3 (Table 1 lists the model acronyms, their main references, and further information, e.g., on spin-up times). Since the same ocean ecosystem model PISCES was used in two different Earth System Models, we analyze a total of 9 different simulations. In most simulations, the ecosystem model was embedded into a coupled climate model and integrated over thousands of years in order to spin-up the model under pre-industrial conditions (see Table 1). In two simulations (REcoM2 and PlankTOM5.3), the ecosystem model was used within a forced ocean model and was initialized with observed climatologies. In these simulations, a control run showed considerably smaller drift than the climate change response. We do not correct the small drift in these models to keep the internal mechanisms in the models consistent.

We describe the most important features of the ecosystem models in the following, and give the full equations and parameters for the offline calculations shown in this work in the Appendix A. The ocean ecosystem models used in this study are structurally similar, but they differ substantially in their details (see Table 2 for an overview of the model structures). Within our selection, all models simulate at least two phytoplankton PFTs, usually representing diatoms and a nanophytoplankton type, and one zooplankton PFT. BEC and TOPAZ have an additional diazotrophic phytoplankton PFT. Moreover, TOPAZ differentiates between diatoms and other large phytoplankton depending on the availability of silicic acid. In PELAGOS, the nanophytoplankton type is further divided into flagellates and picophytoplankton. PlankTOM5.3 includes an explicit coccolithophore type, while in most other models coccolithophores are modeled implicitly as a fraction of nanophytoplankton. Regarding zooplankton PFTs, TOPAZ only has implicit zooplankton activity, diat-HadOCC, BEC, and REcoM2 have one zooplankton type, while PISCES and PlankTOM5.3 differentiate between micro- and mesozooplankton. MEM and PELAGOS have three zooplankton types, i.e., in addition to the micro- and mesozooplankton, they include predatory zooplankton in MEM and heterotrophic flagellates in PELAGOS. Finally, PELAGOS is the only model that includes heterotrophic bacteria explicitly.

2.2 Analysis of NPP and its drivers

A change in NPP can be driven by (i) a change in the biomass specific rate of photosynthesis, (ii) changes in autotrophic respiration, or (iii) changes in phytoplankton biomass through, e.g., zooplankton grazing, sinking and other loss processes of phytoplankton. However, only PELAGOS and REcoM2 model photosynthesis (gross primary production, GPP) and autotrophic respiration separately. Rather, most models calculate NPP directly as the product of the growth rate μ and biomass of phytoplankton, P. In these latter models, changes in marine NPP can thus result only from (i) changes in the phytoplankton growth rate and (ii) changes in phytoplankton biomass. In order to disentangle these two main classes of drivers, it is helpful to consider the full mass balance equation for any phytoplankton type P_i:

$$\Gamma(P_i) = (\mu_i \cdot P_i) - \text{grazing} - \text{sinking} - \text{other losses} \tag{1}$$

where Γ is the sum of the time rate of change and the physical processes of advection, convection, and diffusion, and where the first term on the right hand side is NPP. We consider any driver that alters the growth rate μ_i as a bottom-up driver, while those that alter P, i.e., grazing, sinking, and other losses we consider as top-down drivers, even though only grazing is strictly speaking a top down process.

In all models, the growth rate of phytoplankton is parameterized using a multiplicative function of a maximum growth rate $\mu_{\max}$, the temperature limitation T_f and the nutrient and light limitation factors $N_{\lim}, L_{\lim}$, i.e.,

$$\mu = \mu_{\max} \cdot T_f \cdot N_{\lim} \cdot L_{\lim} \tag{2}$$

In all eight models except for diat-HadOCC, the temperature dependence of phytoplankton growth, i.e., T_f is described using an exponential function based on Eppley (1972), albeit with rather different temperature sensitivities (i.e., Q_{10} values, see also Table 3). In diat-HadOCC, phytoplankton growth is independent of temperature. While in most models the same Q_{10} value is used for all phytoplankton PFTs, mesozooplankton has a higher Q_{10} in PISCES and PELAGOS and each PFT and process has its own Q_{10} value in PlankTOM5.3, derived from observations. In REcoM2 an Arrhenius function is used which results in a Q_{10} that decreases with temperature.

The nutrient and light limitation factors have dimensionless values between 0 and 1, with higher values promoting higher growth. All models consider limitation by multiple nutrients, with six out of the eight models applying Liebig's law of the minimum (Liebig, 1840), such that the value of the strongest limiting nutrient sets the total nutrient limitation. Thus, these models do not consider nutrient co-limitation. Exceptions to this are PELAGOS and diat-HadOCC, where nutrient limitation is multiplicative. In all models, nanophytoplankton growth is limited by nitrate and iron, while diatoms are additionally limited by silicic acid. In several models, limitation with respect to phosphate and ammonia is additionally considered (see Table 2). The limitation regarding a specific nutrient is calculated either with Michaelis–Menten functions (Michaelis and Menten, 1913), following optimal uptake kinetics (Smith et al., 2009), or using a cell quota representation of nutrient deficiency, often with strong differences in half-saturation constants. The values of the half-saturation constants and the equations are given in the Appendix A, Table 4 lists the type of nutrient limitation for the different models.

For diat-HadOCC, the full model equations are not available, therefore we cannot describe the light limitation. In all other models light limitation is parameterized based on the work of Geider et al. (1998), Webb et al. (1974) and Platt et al. (1980). Most models (except for MEM) use the following equation:

$$L_{\text{lim}} = 1 - e^{\left(-\frac{\alpha \cdot \theta^{\text{chl}:\text{c}} \cdot \text{PAR}}{\mu_{T,N}}\right)} \tag{3}$$

where the constant parameter α denotes the initial slope of the photosynthesis-irradiance curve, $\theta^{\text{chl}:\text{c}}$ is the chlorophyll to carbon ratio, PAR is the photosynthetically available radiation and $\mu_{T,N}$ is the maximum growth rate multiplied with the temperature effect and nutrient limitation. PISCES models an additional strengthening in light limitation when the mixed layer depth is deeper than the euphotic zone. In PELAGOS, $\mu_{T,N}$ is replaced by a constant p_r for the maximum specific photosynthetic rate. TOPAZ replaces the instantaneous chlorophyll to carbon ratio with a variable ratio that depends additionally on the memory of irradiance over the scale of 24 h (see Appendix A).

MEM uses the function from Platt et al. (1980) for its light limitation:

$$L_{\text{lim}} = \frac{\left(1 - e^{\left(-\frac{\alpha \cdot \text{PAR}}{p_\text{r}}\right)}\right) \cdot e^{\frac{\beta \cdot \text{PAR}}{p_\text{r}}}}{\frac{\alpha}{\alpha+\beta} \cdot \frac{\beta}{\alpha+\beta}^{\frac{\beta}{\alpha}}} \tag{4}$$

where β is a photo-inhibition index and α, p_r, PAR as above.

Note that in most models, temperature and nutrient status influence also the light limitation, such that in addition to the direct effects of temperature and nutrients on the growth rate, there is an additional indirect way through their effect on light limitation (Geider et al., 1998).

Since PELAGOS does not compute NPP directly and also uses a different formulation for the growth limitation terms, it requires a separate analysis: in this model, NPP is calculated for each phytoplankton type by subtracting autotrophic respiration and other loss processes from its GPP, i.e., $\mathrm{NPP}_i = \mathrm{GPP}_i - \mathrm{exudation}_i - \mathrm{respiration}_i - \mathrm{lysis}_i$. GPP is calculated in PELAGOS in analogy to how NPP is calculated in the other models, i.e., using the product of biomass, maximum growth rate, temperature, light limitation and iron and silicic acid limitation. Nitrate and phosphate limitation are accounted for in the exudation and lysis terms. The reason for this differentiation between the various limiting nutrients is to account for internal storage capabilities of the phytoplankton cells (Vichi et al., 2007). To be able to compare PELAGOS to all other ecosystem models within a common framework, we estimated a multiplicative nutrient limitation factor out of temperature, light limitation and the growth rate that was given in the PELAGOS output: $N_{\mathrm{lim}} = \frac{\mu}{\mu_{\mathrm{max}} \cdot T_{\mathrm{f}} \cdot L_{\mathrm{lim}}}$.

Regarding the loss terms for phytoplankton biomass, grazing is considered in all models. But given the large diversity in the complexity and parameterizations associated with the modeling of zooplankton, the role of grazing may differ substantially among the considered models.

Grazing of zooplankton Z on phytoplankton P is calculated as

$$g_Z^P \cdot T_{\mathrm{f}} \cdot \text{food dependence} \cdot Z \tag{5}$$

in all models except TOPAZ, where g_Z^P is the maximum grazing rate of zooplankton Z on phytoplankton P and T_{f} is the temperature limitation. TOPAZ simulates the effects of zooplankton implicitly and the representation of grazing is based on Dunne et al. (2005). Most models employ the same temperature sensitivity for zooplankton as they use for phytoplankton, with the exception of PISCES and PELAGOS, where the mesozooplankton has a higher temperature sensitivity, and PlankTOM5.3, where each PFT has a different Q_{10} value. The food dependence is modeled differently in each model and is shown in Table 5.

2.3 Data processing

Our analysis is based on monthly mean output for all surface ocean variables for the period 2012–2100. In order to facilitate direct comparisons, we regridded the model to a common 180° × 360° grid using the Earth System Modeling Framework (ESMF) regridding routines included in the NCAR Command Language (NCL) version 6.1.2, with interpolation method set to bilinear.

All models provided in the output vertically (0–100 m) integrated net primary production (NPP) and biomass (in carbon units) of all PFTs. Primary production by diatoms and small phytoplankton was not available for PlankTOM5.3, MEM and PELAGOS, and was estimated offline using the product of biomass and growth rate. The temperature limitations and growth rates were recalculated for all models except for PELAGOS and TOPAZ, where the growth rates were given in the model output. The nutrient and light limitation factors were included in the output of BEC, REcoM2 and TOPAZ, while they were recalculated from the monthly mean data for all other models using the original (not interpolated) data. The equations used for the recalculations are given in the Appendix A. A comparison of recalculated and true values in the BEC showed that the error in the recalculation is on the order of less than 10 %.

Changes for all properties are computed by first averaging the data for two 20 year periods, i.e., 2012 through 2031 and 2081–2100, and then taking the difference. For the growth limitation factors, we show the ratio changes, i.e., for any limitation factor x, we show the ratio $\frac{<x>(t=2081\text{–}2100)}{<x>(t=2012\text{–}2031)}$, where the chevrons denote temporal averages. This is because the product of the relative changes in the temperature, light and nutrient limitation results approximately in the relative change in growth rate, and the factor with the strongest change also has the strongest effect on the change in growth rate.

3 Model evaluation

Most of the models analyzed in this study have been evaluated individually in their respective documenting publications (see references in Table 1). Therefore, we restrict ourselves to an evaluation of the variables that are most relevant for this work, i.e., vertically integrated net primary production (NPP), chlorophyll (chl), surface NO_3, surface PO_4 and surface SiO_3 (Fig. 1 and Tables 7, 8). We compare modeled NPP, using a 1998–2007 climatology for each model, with results from the updated Carbon-based Production Model-2 algorithm derived from SeaWiFS satellite data (Westberry et al., 2008), downloaded from http://www.science.oregonstate.edu/ocean.productivity/index.php. For chlorophyll, we use chlorophyll *a* from the Sea-viewing Wide Field-of-view Sensor (SeaWiFS) Project generated by the NASA Goddard Space Flight Centre (http://oceancolor.gsfc.nasa.gov/SeaWiFS/). We used monthly means computed from Level 3 binned daily products. For both NPP and chlorophyll data we removed coastal values (depth < 500 m) prior to the calculations. For the nutrients, we used the respective objectively analyzed climatologies from the World Ocean Atlas 2013 (Garcia et al., 2014) and compared it to model output for the 1990–1999 period.

On a global scale, the model simulated nitrate fields correlate reasonably well with the observations, with all models showing correlations between 0.61 and 0.85 and normalized SD (NStdDev) between 0.86 and 1.10. However, the bias is rather large, with values between −0.69 and +4.89 $\mathrm{mmol\,N\,m^{-3}}$, corresponding to a bias of approximately −10 to +72 % of the global average. For phosphate (not shown), the results are very similar to those of nitrate, but for silicic acid the models perform less successfully. The correlations are lower and between 0.5 and 0.75, the normalized SD scatter more, and the biases are larger (see Table 7).

The correlations for chlorophyll are mostly between 0.5 and 0.72, however the normalized SD are rather low (most models have NStdDev values < 0.5). The higher SD in the observations stems mostly from the coastal ocean (SD decreases from 1.8 to 0.5 $\mathrm{mg\,Chl\,m^{-3}}$ when removing coastal areas with water depths < 500 m). Most models capture the lower open ocean variability, however in the two models that have a variability comparable to the observations (diat-HadOCC and PlankTOM.3), the variability arises from the open ocean and is therefore significantly higher than the observed open ocean variability.

Least well simulated is the distribution of NPP. The correlations are relatively low (0.17–0.69), the range of normalized SD is as large as that of silicic acid (0.78 to 1.49), and in some of the models, the bias is very large (-8.8–$+6.8\,\mathrm{mol\,C\,m^{-2}\,yr^{-2}}$). Global annual NPP ranges between 17 and $83\,\mathrm{Pg\,C\,yr^{-1}}$ ($40.1\,\mathrm{Pg\,C\,yr^{-1}}$ in the multi-model mean), compared to on average $50.7\,\mathrm{Pg\,C\,yr^{-1}}$ in the satellite-based estimates (Carr et al., 2006) and 58 ± 7 based on ^{14}C NPP (Buitenhuis et al., 2013a). Thus only few models fall within the 95 % confidence interval of the observed NPP.

However, global correlations in nutrients and NPP are strongly influenced by the globally dominant gradient between the Southern Ocean and the low latitudes. While this gradient is generally well reproduced by the models, the model skill in reproducing the regional nutrient and NPP patterns is considerably lower (not shown).

4 Global-scale changes

4.1 Changes in primary production

Starting from very different levels, the models simulate global net primary production (NPP) to change under the RCP8.5 scenario anywhere from -15 to $+30$ % (-4.3 to $+10\,\mathrm{Pg\,C\,yr^{-1}}$) over the 2012 to 2100 period (Fig. 2). One model shows an increase, five models show a decrease and three models project changes less than 1 %, which are not significant (p value < 0.05) when compared to the level of inter-annual variability. The models suggest a median decrease of -7.2 % with an inter quartile range (IQR) of 13.4 % ($-2\,\mathrm{Pg\,C\,yr^{-1}}$ with an IQR of $4.5\,\mathrm{Pg\,C\,yr^{-1}}$). This is comparable to the results reported by Bopp et al. (2013) using 10 Earth System Models from the CMIP5 project under RCP8.5 ($-8.6\,\% \pm 7.9\,\%$) and also to another recent multi-model comparison conducted by Steinacher et al. (2010) under SRES A2 emission scenario ($-10 \pm 3\,\%$, $-2.9 \pm 1.4\,\mathrm{Gt\,C\,yr^{-1}}$). However, the range of projections covered by our study with respect to NPP (45, 16 % without PlankTOM5.3) is higher than the 14 and 6 % reported by Bopp et al. (2013) and Steinacher et al. (2010), respectively.

The regional pattern of the multi-model median change in NPP (Fig. 3b) shows distinct regional differences. The multi-model median suggest NPP increases in the Southern Ocean (south of 40° S, +10 %), in the Arctic Ocean (+40 %), in the southern Indian Ocean and in the southern subtropical Pacific, while decreases by $-10.9 \pm 23.5\,\%$ are projected for the low latitudes (30° S–30° N), with strongest decreases in the North Atlantic (−30 %) and along the Equator in all basins. The range of NPP projections in different regions is given in Table 6. In most models as well as in the multi-model median, the decreases in the low latitudes are stronger than the increases in the high latitudes, resulting in the global decrease in NPP. This partial regional compensation was equally noted by Bopp et al. (2013) and Steinacher et al. (2010). However, these changes are spatially heterogeneous and the multi-model mean masks differences between the individual models.

To illustrate these inter-model differences, we show the IQR (Fig. 3c) of the absolute change in NPP at each location. The IQR of NPP is around $1\,\mathrm{mol\,C\,m^{-2}\,yr^{-1}}$ in the high and intermediate latitudes, which is of the same magnitude as the trends in the multi-model median changes. In the low latitudes the IQR is significantly higher with values between 3 and $5\,\mathrm{mol\,C\,m^{-2}\,yr^{-1}}$, exceeding the multi-model median substantially. Thus, the model projections lack consistency, confounding direct interpretation of the multi-model median response. Rather, it behooves us well to understand the reason for the differences.

4.2 Changes in bottom up vs. top down control

The changes in NPP in the different models can be driven either by changes in the growth rates (bottom-up) or phytoplankton biomass (top-down control) (see Sect. 2.2 above). In order to obtain a first impression of the potential reasons underlying the NPP changes, we split the change in NPP into a component representing the change in the biomass of the whole phytoplankton community and a component representing the whole community growth rate. As the growth rates are only available at the surface in many models, we calculate the components for surface NPP changes. We computed these two components by first calculating a first order Taylor decomposition of NPP into the changes in growth rate weighted with biomass and the changes in biomass weighted with growth rate within each model and for each phytoplankton PFT j:

$$\frac{\delta \mathrm{NPP}}{\delta t} = \sum_j \left(\frac{\delta \mathrm{Biomass}}{\delta t} \Delta \mathrm{Growth} \right)_j + \sum_j \left(\frac{\delta \mathrm{Growth}}{\delta t} \Delta \mathrm{Biomass} \right)_j + \mathrm{Residual}$$

We then determine the median across all models (Fig. 4). We find that the multi-model median growth rates increase nearly everywhere, while the median biomass decreases in the low latitudes, but increases in the Southern Ocean, mimicking the changes in NPP. As was the case for NPP, the model spread is large for both factors driving NPP, and particularly so in the low-latitudes (not shown).

We focus next on the drivers affecting the growth rates, i.e., the bottom up factors temperature, light, and nutrients and do so from a global perspective. To understand the factors affecting phytoplankton biomass, we go deeper into the individual phytoplankton PFTs. This is best done at the regional scale, across which the responses are relatively homogeneous in contrast to the global scale. We analyze and discuss regional changes in Sect. 5.

4.3 Global analysis of bottom up factors

Figure 5 shows the projected changes in sea surface temperature, photosynthetically active radiation (PAR) and surface concentrations of NO_3 and Fe as a zonal average for all models. Figure 6 shows the resulting relative changes in temperature, light and nutrient limitation factors, for all models where the equations describing the limitation factors were available. Note that an increase in any limitation factor corresponds to an alleviation of this limitation i.e., a positive impact on the growth rate. To simplify the plot, for each model only the values for the phytoplankton PFT with the strongest temperature (or light or nutrient limitation factor) response is shown, and minor phytoplankton PFTs like diazotrophs are not included.

In the low latitudes, sea surface temperature is relatively consistently projected to warm by about 2–3 °C (Fig. 5a). In the Southern Ocean, the warming is less pronounced and even more consistent among models (+1 ± 1 °C), while in the Arctic Ocean, the warming is not only stronger but also differs strongly among the models (projections range between no change and +4 °C). This surface ocean warming stimulates phytoplankton growth everywhere and in all models, although given the different temperature sensitivities and the different levels of warming, the spread is large (Fig. 6a). In the low latitudes, the surface ocean temperature limitation factor is simulated to increase by +10 and +30 % (corresponding to weaker limitation). In the Southern Ocean the increase remains small (0–10 %) reflecting the small temperature changes, while in the Northern high latitudes the temperature limitation factor increases by up to 40 %.

In contrast to the large changes in temperature, the photosynthetically active radiation (PAR) at the surface changes little globally, with the important exception of the high latitudes (Fig. 5b), where light availability is affected by changes in sea-ice. In the Arctic, PAR is modeled to increase (projections range between 2 and 18 $\mathrm{W\,m^{-2}}$ increase), while in the Southern Ocean, models disagree even on the direction of change, reflecting the divergent trends in sea-ice (Mahlstein et al., 2013). Consequently, most models show little changes and also little spread in the surface light limitation term between 60° N–60° S (Fig. 6b). In the high latitudes the spread is generally larger, with projections in light limitation factor ranging between −10 and +40 %. However, in all but one model, relative changes in light limitation are of similar magnitude like the relative changes in temperature limitation in the high latitudes.

The iron concentrations are projected to change in a latitudinally relatively uniform manner with changes between −0.05 and +0.2 $\mu\mathrm{mol\,Fe\,m^{-3}}$, with one exception (diat-

HadOCC), where a strong increase is simulated (+0.5 μmol Fe m^{-3}) in the Arctic. These generally small and uniform changes are reflecting the constant dust deposition in all models. Regionally, models differ most in the change in iron concentration in the equatorial Pacific (not shown), probably related to the differences in transport of iron rich water to the Equatorial Undercurrent (Vichi et al., 2011a; Ruggio et al., 2013). There is little agreement among the models with regard to the direction of changes in the surface concentration of nitrate, with decreases and increases of up to ±3 mmol N m^{-3}. Similar changes are modeled for phosphate (not shown). The large range of projected changes leads to very wide ranges for the relative changes in the nutrient limitation factor. In fact, with changes up to ±90 % in the low latitudes and ±15 % changes in the Southern Ocean and 0 and −40 % change in the region north of 30° N, the nutrient limitation factor is changing the most.

In most models, the magnitude of the nutrient limitation term is determined solely by the most limiting nutrient (Liebig limitation, see Sect. 2). Except for PlankTOM5.3, the limitation patterns for different PFTs within the same model are rather similar, but the differences between models are large. Therefore, we show in Fig. 7 the limitation pattern only for diatoms.

In the Southern Ocean, most models agree on iron limiting phytoplankton growth in the annual mean, while PlankTOM5.3 only simulates iron limitation in parts of the Southern Ocean and near the Antarctic continent in summer. In the low latitudes, models show substantial differences in the equatorial upwelling region in the Pacific. Only some models capture the iron limitation shown in data (Moore et al., 2013a). There is substantial variation in the extent of the iron limited region and also the direction of change in iron concentration. As this is a region with high NPP values in the annual mean (see Table 6), uncertainties in this region significantly affect the range in NPP projections. In the remaining low latitudes, models show either phosphate or nitrate limitation.

As half of the models use specified N : P Redfield ratios instead of modeling an explicit PO_4 tracer, nitrate and phosphate limitation cannot be distinguished in these models. However, as nitrate and phosphate are usually highly correlated, a differentiation between nitrate and phosphate limitation might not significantly increase the uncertainty in nutrient limitation projections. In fact, most models agree on stronger nutrient limitation (a decrease in the nutrient limitation factor of between −0.01 and −0.05) in the low latitudes excluding the equatorial upwelling region. The exceptions are REcoM2 and PlankTOM5.3, which simulate weaker nutrient limitation.

In summary, the changes in nutrients and temperature emerge as the most important determinants for the changes in the growth rates, with light generally playing a lesser role, except for the very high latitudes, particularly the Arctic. With these changes in the bottom up controls, we can explain a substantial fraction of the model simulated changes in NPP across the different models. But changes in phytoplankton biomass are clearly relevant as well in explaining some part of the changes in NPP, requiring us to discuss changes in top down controls as well.

5 Regional changes and their drivers

In the following, we will focus our analysis of the bottom-up and top-down drivers of NPP changes and the relative contributions by the different PFT on two example regions, the low latitudes (30° S–30° N) and the Southern Ocean (50–90° S). The low latitudes have been chosen because they explain a large part of the global NPP change (Table 6). Moreover, they exhibit the highest interquartile range (Fig. 3c) and are therefore the main reason for the high range in global NPP projections. The Southern Ocean has been chosen to demonstrate the mechanisms underlying NPP changes for a region where NPP increases in the multi-model median. The drivers of the NPP changes in the North Atlantic and North Pacific will be described briefly at the end of this Section.

Note that we analyze here only the changes in surface NPP, not depth-integrated NPP, because in several cases the separation of NPP in contributions of different PFTs as well as the drivers of NPP changes could only be recalculated for the surface ocean.

However, tests with models where the 3-D limitation factor fields were available (BEC, REcoM2) showed that the mechanism responsible for changes in surface NPP was the same also for changes in depth-integrated NPP. In addition, changes in both original and recalculated surface NPP are strongly correlated to changes in integrated NPP in all models and ocean basins except for the Arctic Ocean (not shown).

5.1 Low latitude NPP changes

Almost all models analyzed in this study agree on an average decrease in surface NPP between the 2012–2031 and the 2081–2100 average in the low latitudes (Fig. 8), albeit with different magnitudes (between –0.004 and –0.09 $\mathrm{mol\,C\,m^{-3}\,yr^{-1}}$). The one notable exception is PlankTOM5.3, which shows a strong increase of on average 0.1 $\mathrm{mol\,C\,m^{-3}\,yr^{-1}}$. In BEC, TOPAZ and diat-HadOCC, the trend is caused by similar decreases in both diatom and nanophytoplankton NPP. In both PISCES simulations, diatom changes contribute about a third of total NPP changes and in PELAGOS and MEM the decrease is mainly driven by a decrease of the NPP by nano- or picophytoplankton, with little changes in diatom NPP. In REcoM2, diatoms and nanophytoplankton trends almost fully compensate each other. The PlankTOM5.3 trend is caused by an increase in coccolithophore NPP (+0.14 $\mathrm{mol\,C\,m^{-3}\,yr^{-1}}$), partly compensated by a decrease in nanophytoplankton NPP (–0.04 $\mathrm{mol\,C\,m^{-3}\,yr^{-1}}$). Changes in diazotrophs (modeled in BEC and TOPAZ) and large non-diatom phytoplankton contribute less than 10 % to the total trend.

Figure 9 shows the relative change in temperature effect, light and nutrient limitation, growth rate, biomass and NPP for diatoms, nano- or picophytoplankton and coccolithophores in the low latitudes. Diat-HadOCC could not be included in the figure as the equations for the limitation factors are not available. Seven out of the eight models agree on an average decrease in NPP and biomass in the low latitudes, but there are two different mechanisms behind this decrease.

The first mechanism is a net decrease in phytoplankton growth rate caused by intensified nutrient limitation. The increase in temperature cannot compensate the decrease in nutrient limitation factor and the result is a decrease in the specific growth rate. Biomass also decreases, driven by the decrease in growth rate and potentially stronger grazing (which will be discussed below). As a result NPP decreases. This mechanism is found in the two simulations using PISCES as ecosystem model for both diatoms and nanophytoplankton and for the diatoms in the BEC. As diat-HadOCC does not have a temperature dependence, the NPP decrease in diat-HadOCC is potentially also driven by stronger nutrient limitation, however the potential contributions of light limitation cannot be shown.

In six models the NPP decrease is caused by a second mechanism: the increase in nutrient limitation is outweighted by the increase in temperature, leading to a net increase in the specific growth rate. The observed decrease in NPP is thus not bottom-up driven, but caused by a loss of biomass. Possible reasons for the biomass loss are (1) changes in circulation or mixing leading to a stronger lateral/vertical loss of biomass, (2) increased aggregation or mortality of phytoplankton if explicitly modeled or (3) a higher grazing pressure.

We hypothesize that the loss of biomass caused by physical transport does not significantly increase, as all models show an increase in stratification over the next century. Furthermore, phytoplankton aggregation (and mortality) depend exponentially (linearly) on biomass but are temperature independent, so neither aggregation nor mortality losses can increase at lower biomass levels. This leaves us with increased grazing pressure as the most likely driver of the biomass loss in the low latitudes.

This hypothesis is supported by the fact that in all five models, for which the grazing fluxes were available, the fraction of grazed NPP increases throughout the 21th century (Fig. 10), i.e., the grazing pressure increases. In TOPAZ the increase is comparatively small (+0.1 %). However, grazing is the only loss process in this model and changes in the ratio between grazing and NPP ratio are directly translated into either biomass changes or changes in physical transport. In the models where aggregation and mortality are explicitly modeled, the increase in the grazed fraction of NPP is stronger (+5 ± 3 %). However, with decreasing phytoplankton biomass the aggregation losses must decrease in these models, at least partly compensating the increase in grazing. Unfortunately, the mortality and aggregation fluxes as well as the loss of biomass caused by physical transport have not been stored in the model output. Recalculated values are not precise enough to analyze the difference between NPP and loss processes. Therefore we cannot further differentiate our analysis into the changes in mortality, aggregation and physical biomass loss. A more detailed analysis of the loss fluxes is beyond the scope of this work but is planned in subsequent work.

To understand the potential drivers for the increase in grazing pressure between the present and the future scenario, we analyze the fraction of NPP that is grazed by zooplankton, given by:

$$\frac{\text{grazing}}{\text{NPP}} = \frac{g_Z^P \cdot T_\mathrm{f} \cdot P\text{-dependence} \cdot Z}{\mu_\mathrm{max} \cdot N_\mathrm{lim} \cdot L_\mathrm{lim} \cdot T_\mathrm{f} \cdot P} \tag{6}$$

Here, g_Z^P is the grazing rate, T_f the temperature limitation, P and Z denote phytoplankton and zooplankton biomass and μ_max the maximum phytoplankton growth rate, as introduced in Eqs. (2) and (5). Climate change affects the ratio between grazing and NPP via temperature and also via changes in nutrient and light limitation. Furthermore, the grazing : NPP ratio is affected by changes in zooplankton biomass, i.e., increases in total grazing and zooplankton mortality indirectly play a role. In the models where the same temperature function for both phytoplankton growth and zooplankton grazing is used (see Table 3), the temperature limitation T_f cancels out. Still, with a higher temperature the total grazing increases due to an increase in zooplankton growth rate and thus an increase in zooplankton biomass, which will intensify grazing (see Eq. 6). On the other hand, grazing pressure can increase through a decrease in the phytoplankton growth rate μ, because of stronger light or nutrient limitation, thus decreasing NPP in the equation above.

To understand the drivers of the observed changes in grazing pressure, we compared the effects of changes in temperature and nutrient limitation on grazing in a one-box model simulating growth and biomass of one phytoplankton, NPP, grazing and zooplankton biomass based loosely on the equations and parameterizations of the BEC. We did not include further phytoplankton loss terms like aggregation or mortality and used a quadratic temperature-independent mortality as loss process for zooplankton. We performed a spin-up until the model reached an equilibrium state under conditions representative for the low latitudes (temperature limitation of 0.8 corresponding to about 27 °C, strong nutrient limitation of 0.1 corresponding to less than $0.5\,\mathrm{mmol\,NO_3\,m^{-3}}$ and weak light limitation). As grazing is the only loss process of phytoplankton, 100 % of NPP are grazed in the equilibrium state. To test the sensitivity of grazing pressure to temperature changes, we increased the temperature from 27 to 30 °C over a time period of 10 years but kept light and nutrient limitation constant. The experiment showed an 8 % decrease in phytoplankton biomass within the 10 simulation years even though the phytoplankton growth rate was increasing, caused by a temperature-driven increase in zooplankton biomass and thus grazing. On average, about 101 % of NPP was grazed per month during the 10 year period.

To test the sensitivity of grazing pressure to nutrient changes, we enhanced nutrient limitation by 30 % (nutrient limitation factor decreases from 0.1 to 0.07) over 10 years while keeping temperature constant at 27 °C. In this experiment, phytoplankton biomass decreased by 15 %. Besides the decrease in phytoplankton growth in this experiment compared to the equilibrium state and the first experiment, 102.5 % of NPP was grazed on average each month, indicating that the change in nutrient limitation has a similar effect on grazing like the temperature increase. These results indicate that the grazing pressure is increased by both stronger nutrient limitation and higher temperatures. As the basic structure of the NPP and grazing equations is similar in most models, this mechanism might explain the observed biomass loss in the low latitudes. However, the specific grazing parameterizations and also the zooplankton mortality parameterizations differ substantially between models, such that the strength of the grazing response and the magnitude of the biomass loss is most likely different between models.

Regarding the increase in NPP in PlankTOM5.3, we note that export production changes do not follow the increase in NPP but decrease strongly (not shown). There is an increase in microzooplankton biomass and grazing on phytoplankton, leading to an increase in regenerated production, even as new production decreases. We conclude that the increase in nutrient concentration, which causes the NPP increase is not driven by higher nutrient input but by increased recycling of nutrients.

In summary, while the majority of the models simulate a decrease in NPP in the low-latitudes, only in three of these models is the decrease caused by lower phytoplankton growth due to an enhanced nutrient limitation, intensified by increases in grazing pressure. In the other models, the low-latitude decrease in NPP is a consequence of a loss of phytoplankton biomass, most likely as a consequence of a relative increase in grazing, part of which is driven by higher growth rates for zooplankton permitting them to impose higher grazing pressures on phytoplankton.

5.2 Southern Ocean NPP changes

All models simulate an increase in surface NPP in the Southern Ocean south of 50°, but the magnitude of the change varies by several orders of magnitude (+0.006 and +0.11 $\mathrm{mol\,C\,m^{-3}\,yr^{-1}}$, Fig. 11). Also the contributions of the different phytoplankton PFT to these NPP trends differ strongly between the different models. Four models show a stronger increase in the NPP by nanophytoplankton compared to that by diatoms, two models show an exclusively diatom-driven NPP change and two models show similar changes in the NPP by diatoms and nanophytoplankton. Only one model shows a significant decrease in diatom NPP.

Across all models for which the limitation factors could be analyzed, the increases in NPP are largely driven by an increase in the growth rates, supported in most, but not all models by an increase in phytoplankton biomass (Fig. 12). Models also agree that warming is an important driver for the enhanced growth (2–12 % increase). In addition, all but the CNRM/PISCES model show a relief from nutrient stress, i.e., an increase in the nutrient limitation factor (1–15 % increase), although these models remain iron limited throughout the 21st century. In contrast, there is no agreement on the direction of change in light limitation, with three models showing an increase (+2 to +6 %) and five models a decrease (−0.1 to −20 %).

Considering the combined effects of temperature, light and nutrient limitation, it turns out that surface ocean warming is the most important driver for the increase in phytoplankton growth in seven out of eight ecosystem models. Smaller relative changes in light and nutrient limitation factor modify the temperature-driven increase in growth. REcoM2 is the only exception. In this model, a strong increase in nutrient limitation factor and a strong decrease in light limitation factor result in a moderate increase in growth rate, with temperature effects playing a comparatively small role.

In most models the increase in growth rate is associated with an increase in biomass. However, in BEC, TOPAZ and REcoM2, the biomass of nanophytoplankton biomass decreases despite increases in their growth rate. As was the case for the low latitudes, this net biomass loss in the presence of enhanced growth must be caused by an increase in loss processes (e.g. grazing, aggregation, mortality). The top-down control causes even a small decrease in nanophytoplankton NPP in these models.

In summary, all models analyzed in our study agree on increases in phytoplankton growth rate and NPP in the Southern Ocean, and seven out of eight models agree on temperature being the strongest driver, with nutrient and light limitation often having opposing tendencies. Thus, there is currently higher agreement among models regarding changes in the Southern Ocean than in the low latitudes, with changes in light limitation being the main uncertainty in the Southern Ocean.

5.3 Northern Hemisphere NPP changes

In the following we give a brief overview on the drivers of NPP changes in the North Atlantic and North Pacific. We do not discuss the Arctic Ocean, as in the Arctic changes in surface NPP are not well correlated with changes in integrated NPP in many models, therefore the drivers of surface NPP changes are presumably not the driver for integrated NPP change. An analysis of Arctic Ocean NPP changes has been recently published by Vancoppenolle et al. (2013).

In the North Pacific, models do not agree on the direction of the NPP change, with PlankTOM5.3, MEM, TOPAZ, CNRM/PISCES and REcoM2 suggesting increases and diat-HadOCC, BEC, IPSL/PISCES and PELAGOS suggesting decreases, resulting in almost no change in the multi-model median. Most models follow the same mechanism that they exhibit in the low latitudes. The main difference is a larger temperature increase and a weaker decrease or even increase in the nutrient limitation factor. For the models following the classical stronger nutrient limitation mechanism, this results in a weaker decrease in growth rate and slightly weaker decreases in biomass. For the models that are mainly driven by temperature and top-down control, the increase in growth rate is stronger compared to the low latitudes while the decrease in biomass is comparable, leading in some models to an increase in NPP. Overall, the changes in growth and biomass are strongly diverging in the temperature and top-down control driven models.

In the North Atlantic, all models agree on a decrease in NPP except for PlankTOM5.3, which shows a small increase. Most models show a decrease in growth rate, at least in the PFT causing the overall NPP trend, driven by lower nutrient availability. The effects of changes in light limitation are in most models insignificant, while REcoM2 and both PISCES simulations show a small increase in light availability. The decreases in growth rate are followed by decreases in biomass in all models. However, particularly the models that are temperature and top-down control driven in the low latitudes show a strong decrease in biomass compared to the decrease in growth rate, suggesting additional effects of stronger top-down control.

6 Discussion

6.1 NPP changes and their drivers

Our finding of temperature playing a key role in defining the response of marine NPP to future climate change contrasts with the conclusion of the majority of the past studies, which attributed the decrease in NPP to a decrease in nutrient availability, particularly in the low latitudes (Bopp et al., 2001; Moore et al., 2002; Steinacher et al., 2010; Marinov et al., 2010). To explain this discrepancy, we focus on the temperature and nutrient functions in the models used in the studies above.

In Steinacher et al. (2010) and Bopp et al. (2001), NPP trends in a total of 6 ecosystem models were analyzed. These models were HAMOCC5.1, HAMOCC3, NCAR CSM1.4-carbon, CCSM3/BEC and an earlier version of IPSL/PISCES. HAMOCC5.1 has no temperature dependence of phytoplankton growth at all, so that only nutrient and light limitation are considered.

In HAMOCC3 and NCAR CSM1.4-carbon, the temperature limitation function for phytoplankton growth has a Q_{10} value of 1.13 for temperatures higher than 15 °C, resulting in a very low temperature sensitivity in the low latitudes. It is thus not surprising that ocean warming did not significantly affect global productivity in these model simulations compared to the models analyzed in this study that have a Q_{10} of at least 1.68.

The third model analyzed by Steinacher et al. (2010) is the IPSL model with PISCES as the ecological/biogeochemical component. A later version of this model is analyzed in our study. Consistent with Steinacher et al. (2010) we find that changes in nutrient limitation are the main driver of NPP changes in PISCES, independent of the Earth System Model to which it is coupled. While the change in temperature effect is comparable to the other models analyzed in our study (+20 % increase in IPSL, +14 % in CNRM), the relative decrease in the nutrient limitation factor is much stronger here (−45 % in IPSL, −35 % in CNRM).

As the total change in nutrient limitation is not bigger than in other models, the strong relative change must be caused by a stronger nutrient limitation owing to low nutrient concentrations at the beginning of the simulations. Indeed, the PISCES models tend to have a negative bias, i.e., too low nutrient concentrations in the low latitudes ($-0.63\,\mathrm{mmol\,N\,m^{-3}}$ and $-0.18\,\mathrm{mmol\,P\,m^{-3}}$ for IPSL/PISCES and $+6.15\,\mathrm{mmol\,N\,m^{-3}}$ and $-0.23\,\mathrm{mmol\,P\,m^{-3}}$ for CNRM/PISCES). PISCES has rather low half-saturation constants (equivalent to weak nutrient limitation) compared to other models in our study. We hypothesize that because of the low half-saturation constants in PISCES, nutrients are used very efficiently, causing a very low initial concentration in the limiting nutrient after the spin-up. A further decrease of this low initial nutrient concentration caused by climate change will result in very strong changes in relative nutrient limitation that outweigh the warming effect.

Finally, the CCSM3/BEC model analyzed in Steinacher et al. (2010) had the same temperature dependence as the version of BEC used in our study (coupled to CESM1). They found a weak decrease in global NPP under the SRES A2 scenario and attributed it to the general decrease in nutrient availability. Marinov et al. (2013) also report a supposedly nutrient driven decrease in NPP for the 21st century under the SRES A2 scenario using BEC coupled to CCSM3.1. But our analysis shows that the global NPP decrease, and particularly that in the low latitudes, is not caused by decreasing growth rates, such as one would expect from increasing nutrient limitation. Rather the decrease in NPP is caused by biomass losses, presumably a result of a warming-induced increase in grazing pressure.

To summarize, in many of the studies where the NPP decrease is nutrient driven, the temperature effect was either a lot weaker than in the ecosystem models used here, or not considered at all. Moreover, usually climate change scenarios were used in which the temperature increase was lower than under RCP8.5 used here. This indicates that the temperature effect might have been underestimated.

Our identified importance of warming for future NPP is more in line with another group of studies, where global NPP was projected to increase with climate change, and a temperature-driven increase in metabolic rates was identified as the cause (Schmittner and Galbraith, 2008; Sarmiento et al., 2004; Taucher and Oschlies, 2011). This agreement might be somewhat fortuitous, as Schmittner and Galbraith (2008) and Taucher and Oschlies (2011) considered only the temperature dependence of phytoplankton growth and remineralization, while the growth of zooplankton and hence the grazing pressure on phytoplankton were independent of temperature. Likewise, the algorithm used to estimate chlorophyll in Sarmiento et al. (2004) is based on the assumption that chlorophyll is purely bottom-up controlled. Therefore, these studies are limited to temperature effects on phytoplankton growth and therefore might overestimate the role of temperature, since they disregard the potential effects of top-down control on NPP.

A similar conclusion can be drawn from the most recent study by Dutkiewicz et al. (2013) where they aimed to separate the direct temperature effect from the altered nutrient input and light availability caused by stratification. In their study, temperature, nutrient and light changes compensate each other nearly perfectly, resulting in very little change in global NPP. But also here, zooplankton growth was assumed to be independent of temperature, likewise neglecting the effect of temperature changes on top-down control.

On the regional level, our results confirm the increase in Southern Ocean NPP reported by several authors (Bopp et al., 2001; Sarmiento et al., 2004; Steinacher et al., 2010; Taucher and Oschlies, 2011; Dutkiewicz et al., 2013). Previous work has focused on sea ice retreat and shoaling of the mixed layer as reasons (Sarmiento et al., 2004; Taucher and Oschlies, 2011; Bopp et al., 2001) as well as temperature-driven increases in growth rate (Dutkiewicz et al., 2013; Steinacher et al., 2010). We show here that in seven out of nine ecosystem models the temperature response is the main driver for the surface NPP increase. In Steinacher et al. (2010), the only model that simulates a decrease in NPP in the high latitudes is the MPIM model which has no temperature dependence, further emphasizing the importance of temperature effects in the high latitudes.

6.2 Changes in phytoplankton community

Seven out of nine models in our study show a global decrease in the relative abundance of diatoms and a spatial pattern with decreases in low latitudes but increases in the Southern Ocean, confirming results reported by Bopp et al. (2005), Marinov et al. (2010), Dutkiewicz et al. (2013), Manizza et al. (2010) and Marinov et al. (2013). However, the drivers for the observed changes are different among models. In the low latitudes, diatoms show a stronger response to nutrient limitation than nanophytoplankton in four models (BEC, MEM, REcoM2, PlankTOM5.3). In the other models, diatoms show a weaker (CNRM/PISCES, TOPAZ, PELAGOS) or almost equal (PISCES) response to nutrient changes compared to nanophytoplankton, but in these models diatoms suffer from higher relative biomass losses than small phytoplankton. In diat-HadOCC, the driver for changes in diatom relative abundance could not be analyzed.

In PlankTOM5.3, all three PFTs exhibit an increase in growth rate. The driver is a temperature increase and, for nanophytoplankton and coccolithophores, a relief from nutrient stress by an increase in the nutrient limitation factor. In contrast, diatoms are increasingly limited by the availability of silicic acid, which diminishes the increase in diatom growth rate. In addition to growth rate changes, nanophytoplankton shows severe relative biomass losses (−50 %). The overall result is a decrease in nanophytoplankton NPP (−40 %), an increase in diatom NPP (+50 %) and a strong increase in coccolithophore NPP (+80 %) in PlankTOM5.3.

In the Southern Ocean, diatoms respond more strongly to changes in nutrient limitation than nanophytoplankton in all models. In addition, 5 models show a significantly stronger biomass loss of nanophytoplankton compared to diatoms, only MEM shows stronger diatom biomass loss. In PELAGOS the diatom fraction is almost 100 % south of 50° S, and shows little changes. The final result is a stronger increase in diatom NPP compared to nanophytoplankton NPP in BEC, TOPAZ, IPSL, CNRM and REcoM2, and a weaker increase in diatom NPP in MEM and PlankTOM5.3.

Title Page
Abstract Introduction
Conclusions References
Tables Figures
◀| |▶
◀ ▶
Back Close
Full Screen / Esc
Printer-friendly Version
Interactive Discussion

In a previous study on changes in phytoplankton composition, the difference between the diatom and nanophytoplankton nutrient response have been identified as the primary driver of the decrease in diatom fraction (Bopp et al., 2005). Likewise, Marinov et al. (2010, 2013) identify differences in nutrient response as an important driver and additionally discuss temperature and light effects.

Our results show that while models currently agree on a global decrease in diatom fraction, there is no agreement on regional changes and models do not agree on the mechanisms behind relative diatom abundance changes.

7 Identifying and reducing uncertainties

The spread in globally integrated NPP projections in our study is 45 %, with the PlankTOM5.3 model causing 25 % of it alone. Given this wide spread in NPP projections, we attempt to identify the different sources of uncertainty in the following and then investigate whether there is a way to narrow the uncertainty of the projections using emergent constraints.

7.1 Sources of model uncertainties

If we want to reduce the spread in NPP projections, we need to understand how much of the uncertainty arises from the physical forcing and how much is caused by the different ecosystem parameterizations. In the following we compare the range in projections of ecosystem models forced with the same Earth System Model with the range in projections of different Earth System Models forcing the same ecosystem model.

In our study, one ecosystem model (PISCES) is forced with two different Earth System Models (CNRM and IPSL, respectively), which differ in their atmospheric component and the spatial resolution of the ocean model. (A detailed discussion of the differences between the Earth System Models can be found in Séférian et al., 2013). The IPSL and CNRM simulations have different nutrient limitation patterns in the equatorial Pacific and the IPSL NPP change in the low latitudes is three times higher than the CNRM change. However, both models have a similar global NPP response to climate change, and they show the same mechanism (relative importance of temperature vs. nutrient effects) for NPP changes in the low latitudes, even though the difference in sea surface temperature change is substantial (1.2 °C).

We do not have a true corresponding case where different ecosystem models were run in the same ocean circulation model and subject to the same atmospheric forcing. However, a comparison of the results from the MEM and REcoM2 ecosystem models, which were run in different ocean circulation models, but with the same atmospheric forcing from MIROC5, suggests highly divergent NPP changes. The projected increase in SST differs by about 1 °C (Fig. 5) and the responses in temperature limitation of biological processes are at the opposite ends of the full range of temperature responses (Fig. 6). Further differences in high latitude light limitation, global nutrient limitation pattern and in loss processes result in about three times stronger NPP changes in MEM and different contributions of the individual PFTs. This large difference in NPP changes indicates that the ecosystem structure and the chosen parameterization are a strong contributor to the projection uncertainty.

Consistent with our results, Bopp et al. (2013) noticed that models using the same marine biogeochemical/ecosystem component in their study (IPSL-CM5A-LR and IPSL-CM5A-MR, MPI-ESM-LR and MPI-ESM-MR, GFDL-ESM2G and GFDL-ESM2M, respectively), project similar changes in globally integrated NPP. Likewise, Sinha et al. (2010) compare simulations of two different circulation models coupled to the same biogeochemical model. They show that differences in the underlying physics lead to substantial differences in PFT biogeography, but only small effects on total NPP. However, these results are based on only a handful of models. For a more solid comparison between differences in ecosystem behavior and uncertainty in the ocean general circulation model one should compare a bigger group of ecosystem models forced with the same circulation model (e.g. Kwiatkowski et al., 2014) and vice versa.

Title Page
Abstract Introduction
Conclusions References
Tables Figures
◀◀ ▶▶
◀ ▶
Back Close
Full Screen / Esc
Printer-friendly Version
Interactive Discussion

Regarding uncertainties introduced by the ecosystem structure and parameterization, the biogeochemical and biological processes that contribute the largest uncertainties are:

- Initial nutrient concentrations: models (except PlankTOM5.3) agree on similar decreases in nutrient concentration in the low latitudes, and also on the total change in the nutrient limitation factor between ±0.1, despite disparities with regard to the identification of the most limiting nutrient. However, the differences in relative nutrient limitation change are very large (±90 %, see Fig. 6). Particularly the PISCES simulations show a strong relative decrease in nutrient limitation, which is caused by low nutrient concentrations at the beginning of the simulation (see Sect. 3). On the other hand, a positive bias in nutrients as observed in other models might lead to a too weak response in nutrient limitation. We emphasize here that the initial nutrient concentration after 1000 years of spin-up simulation is caused by the ecosystem, so this is an uncertainty arising from the coupling of the ecosystem and ocean general circulation models likely with contributions both from the simulation of the biogeochemistry and physics.

- Relative importance of iron vs. nitrate limitation and projections for iron concentrations: increases in iron availability allow the small global increase in nanophytoplankton NPP in REcoM2 and attenuate or even outbalance the low latitude NPP decrease in BEC and TOPAZ. This is of particular relevance in the equatorial upwelling region in the Pacific (see Fig. 3), which is iron limited according to observations (Moore et al., 2013a) and is responsible for 14–33 % of global NPP at present in the different models (Table 6). The differences in the projected changes in iron concentration in the equatorial upwelling region in the Pacific are potentially related to differences in circulation: according to Vichi et al. (2011b) and Ruggio et al. (2013), the Equatorial Undercurrent may intensify and shoal with climate change and this may bring more iron to the eastern equatorial upwelling, partly off-setting the reduced nutrient input due to the warming surface.

Note that the dust deposition is held constant in current projections. Variable iron forcing in future simulations might further increase this uncertainty.

- Different Q_{10} values (between 1.68 and 2.08) and different projections for SST increase (+2, +3 °C) together result in a high uncertainty of the temperature response of both phytoplankton growth and zooplankton grazing. Further uncertainty is introduced by the stronger temperature response of zooplankton types parameterized in some models.
- Different responses of the top-down control and the microbial loop, potentially related to different Q_{10} values and differences in the partitioning of the grazed material.
- There is no agreement with regard to the direction of change in light limitation in the Southern Ocean, reflecting the wide range in projected sea-ice changes and other factors influencing surface light such as cloud cover. However, light limitation introduces currently only a minor uncertainty compared to the nutrient and temperature effects, at least for surface NPP.

We conclude that in addition to the uncertainty introduced by the different ocean circulation models, the structures and parameterizations of the different ecosystem models substantially increase the overall projection uncertainty.

7.2 Constraining NPP projections

The concept of emergent constraints (e.g. Allen and Ingram, 2002) has been used with success to reduce uncertainties for future projections. The basic premise is that models that provide a better fit to a specific set of current constraints provide a better estimate for the future changes. The emergent constrain is usually established by finding a good correlation between an observable parameter for the present and the future change in NPP.

We have tested for correlations between the different models's skill to predict current NPP and their projected changes, using both the 2012–2031 average of globally integrated NPP and the slope between chlorophyll *a* and sea surface temperature as a measure for model skill. Although chlorophyll *a* is a poor indicator for biomass in the low latitudes (Siegel et al., 2013), it can be used as indicator for model skill and is comparatively well constrained by observations. As the metric for the projected changes we used the change in NPP defined as the difference between the 2012–2031 average and the 2081–2100 average and the change in NPP weighted with the temperature increase. Moreover, as regions with positive and negative changes might cancel each other out, leading to little net NPP changes despite strong local changes, we also tested for a relation between absolute NPP changes and model skill.

We did not find any significant correlation between model skill and NPP changes, neither on regional nor global scales, and the relation is weak at best between globally integrated NPP and the absolute change in NPP (Fig. 13).

We hypothesize that the cause for this lack of relationship is the uncertainty in the relative importance of the net effect of temperature on NPP and on nutrient limitation. This hypothesis is supported by results from Taucher and Oschlies (2011) who used two simulations, one temperature dependent and one independent. Both simulations fitted equally well to observations, but the direction of NPP change was opposite. Similarly, while Hashioka et al. (2013) demonstrated that all four marine ecosystem models in their analysis simulate an increase in diatom fraction during the spring bloom for present-day conditions, but are controlled by different mechanisms.

We find that matching the current observations is not sufficient to estimate which sign of future NPP change is more realistic. Thus we need a better understanding of the mechanisms in order to reduce the uncertainty in projections. Efforts to extend the amount of data that is available for model parameterisation and evaluation (Buitenhuis et al., 2013b) will hopefully help achieve that goal.

8 Caveats and limitations

One major difficulty faced in this study is the limited availability of model output variables related to ecosystem growth and loss rates, particularly limitation factors and grazing rates.

The changes in growth rate, temperature limitation, light and nutrient limitation reported in this work have been recalculated in six out of nine models using surface monthly mean fields. The obtained results are therefore an approximation of the original values. We have compared recalculated values with original values in the models where the limitation factors were given, and we estimate the error to be less than 10 %. We conclude that while the absolute values reported might be inaccurate, the relative importance of nutrient vs. temperature limitation shown in this work is correct. Furthermore, we can discuss only surface NPP changes. For the models where 3-D limitation factors were available (BEC, REcoM2), we compared our results for the surface with the 100 m average, and we can confirm that the same mechanisms that govern the surface changes also hold for the 100 m average. In addition, the changes in surface NPP correlate with the changes in integrated NPP in all models, except for the Arctic Ocean. It therefore seems likely that our surface drivers also describe the changes in integrated NPP. However, changes in light limitation might be not constant over the mixed layer and become more important when considering drivers for integrated NPP changes.

A further weakness of our approach is that we treat temperature limitation, nutrient and light limitation separately. In most models however light limitation depends on both temperature and nutrients. Warmer water directly increases the growth rate via the direct temperature effect but in addition potentially decreases the growth rate via increased demand for light. As the changes in light limitation in the low latitudes are much smaller than the changes in temperature limitation and nutrient limitation, we conclude that the indirect effects of temperature and nutrients on light limitation are of minor importance.

The last caveat regards the processes that have been shown to be of relevance for NPP projections yet are not included in current generation of marine ecosystem models.

- Biodiversity has been shown to (positively) influence productivity in trait-based models (Prowe et al., 2012, 2011). The classification into different PFTs is only a very rough estimate of the diversity in the real ocean and can not reflect diversity effects on NPP. Nevertheless, Prowe et al. (2014) show that different diversity representations cause only small global NPP changes in an environmental change experiment.
- There is no influence of changing pH or carbonate chemistry on phytoplankton represented. Ocean acidification will impact biogeochemical cycles and ecosystem processes in many complex ways (Doney et al., 2009), including negative effects on calcification (e.g. Ridgwell et al., 2009), increase of N_2 fixation (Levitan et al., 2007) and changes in the C : N : P ratio (Finkel et al., 2009). The net effect of ocean acidification on phytoplankton growth is currently unclear, though some model results indicate a positive effect on NPP (Tagliabue et al., 2011).
- The nutrient demand is in all models independent of temperature, although temperature has been shown to affect phytoplankton metabolism towards a higher relative NO_3 demand (Toseland et al., 2013), which might further reduce NPP in nitrate limited regions.
- The only direct effect of climate change on zooplankton is temperature. There are no phenological or trophic mismatches, diseases or changes in predation from higher trophic levels. Also, since at maximum only three trophic levels are represented, there are no effects of larger predators or human fishing activity.
- In most models all PFTs follow the same temperature curve. A parameterization of a stronger temperature response of zooplankton could reinforce the decrease in NPP and/or affect the response of the microbial loop.

- Only two models include nitrogen fixation, which might increase NPP in regions with low nitrate concentrations. However, in models where diazotrophs are included they constitute only a small fraction of the changes in total NPP.

Including these processes in marine ecosystem models will make the problem of predicting future NPP changes even more complex and probably further increasew the uncertainty and spread in NPP projections. Nevertheless, there has been substantial progress on these challenges during the last years. Many processes have been analyzed and are now represented in several marine ecosystem models, including varying Chl : C : N : P ratios, a differentiation into an increasing number of PFTs and the consideration of several co-limiting nutrients. The importance of the temperature effect on growth has been analyzed by several authors, which has not even been considered in many models several years ago. Overall, understanding of the future NPP changes has evolved considerably during the last decade even though the projection uncertainty is still high.

9 Conclusions

Our analysis of one of the largest ensemble of marine ecosystem models to date reveals that the current generation of these models exhibits a much larger spread of NPP projections compared to previous studies. Global NPP is projected to change between −15 and +30 % by the end of this century for the high emission scenario RCP8.5, with the largest inter-model discrepancies stemming from the low latitudes. While this large spread confounds direct interpretation of the multi-model median response, it strongly motivates the need for a mechanistic understanding for why the models differ.

Eight out of the nine models simulate either a decrease in NPP or changes less than 0.5 % (seven and one model, respectively) in the low latitudes, but for very different reasons. In five models, the warming-induced enhancement of phytoplankton growth exceeds the increased nutrient limitation, resulting in stronger phytoplankton growth. The decrease in NPP is caused by a substantial decrease in phytoplankton biomass, which is likely a consequence of warming-induced enhanced grazing by zooplankton. In two models, the classical enhanced nutrient limitation process decreases the growth rate in the low latitudes and consequently decreases global NPP. In addition an increased grazing pressure intensifies the NPP decrease in these models. One model does not parameterize temperature effects on growth or grazing, leaving nutrient limitation as most likely driver. The last model simulates actually an increase in NPP in the 21st century, despite a reduction in the net supply of nutrients, as a warming-induced speedup of the microbial regeneration loop permits a much higher retention of the limiting nutrients. In the high latitudes all models project an increase in NPP, largely because of warming stimulating growth. Thus in this set of models, temperature and nutrient concentrations are at least equally important driver for changes in NPP in the low latitudes and the Southern Ocean, contradicting many prior studies that emphasized the sole importance of stronger nutrient limitation.

While we emphasize here the role of temperature, our understanding of how temperature controls the most important ecological and biogeochemical processes is not well established. There are major uncertainties in quantifying the temperature sensitivities of different physiological processes and of functional types (Ikeda et al., 2001; Lomas et al., 2002; Hirst and Bunker, 2003; Hancke and Glud, 2004; Sand-Jensen et al., 2007). Several authors suggest a stronger temperature response of heterotrophs than autotrophs (López-Urrutia et al., 2006; Rose and Caron, 2007), which would lead to major consequences for the metabolic balance of the oceans under rising temperatures (Duarte et al., 2013; Williams et al., 2013; Ducklow and Doney, 2013; García-Corral et al., 2014). Thus, in order to improve our ability to project changes in marine NPP, we need a better understanding of the temperature dependency of all key ecological/biogeochemical processes. In particular, this includes the determination of the different temperature response functions for the different PFTs and trophic levels. Furthermore, further effort should be put into investigating concurrent effects of several limiting factors (i.e. Toseland et al., 2013), and the partitioning of the grazed material into particulate/dissolved organic matter and a fraction that is immediately respired.

In addition, the representation of present day nutrient concentrations and resulting limitation patterns should be further improved. Particularly a bias in present-day nutrient concentration strongly affects relative changes in nutrient limitation and therefore NPP projections.

Furthermore, understanding the reasons for the differences in contemporary NPP estimates and potentially further constraining the parameterization of phytoplankton growth will help to reduce the NPP projection uncertainty. In addition, as zooplankton grazing has shown to be an important driver for NPP changes, emphasis should be put on potential controls on zooplankton that are currently not represented. Zooplankton mortality, for example, is often parameterized as a linear or quadratic closure term that has been shown to have a strong influence on zooplankton biomass (Edwards and Yool, 2000).

To ease future studies of NPP changes, we recommend inclusion of mixed layer averages of growth rate, light and nutrient limitation and grazing fluxes in the model output. The availability of changes in growth rates could prevent common misinterpretations of drivers by analysing univariate correlations with only one of several possible drivers. We demonstrate that mechanisms found in one model are often not transferable to another model and sometimes not even between different versions of the same model. Results of model comparison studies strongly depend on the choice of model and can not be used to explain changes in a model that has not been part of that study.

Finally, our analysis has revealed that our current ability to project future changes in marine NPP is relatively poor and smaller than had been suggested by previous studies that looked at a smaller and also less diverse set of marine ecosystem models. Thus, great care must be taken when using any given model projection for determining

Title Page
Abstract Introduction
Conclusions References
Tables Figures
◀◀ ▶▶
◀ ▶
Back Close
Full Screen / Esc
Printer-friendly Version
Interactive Discussion

how the changes in NPP impact other marine ecosystem services, such as fish yield and others.

Appendix A: Model equations and parameters

A1 BEC

Growth rate of phytoplankton PFT *i*

$$\mu^i = \mu^i_{\max} \cdot T_f \cdot N^i_{\lim} \cdot L^i_{\lim}$$

Temperature function (for all PFTs)

$$T_f = Q_{10}^{\frac{T-T_{\mathrm{ref}}}{10}}$$

Total nutrient limitation

$$N^{\mathrm{nano}}_{\lim} = \min\left(N^{\mathrm{nano}}_{\mathrm{Fe}}, N^{\mathrm{nano}}_{\mathrm{PO_4}}, N^{\mathrm{nano}}_{\mathrm{NO_3+NH_4}}\right)$$

$$N^{\mathrm{diat}}_{\lim} = \min\left(N^{\mathrm{diat}}_{\mathrm{Fe}}, N^{\mathrm{diat}}_{\mathrm{PO_4}}, N^{\mathrm{diat}}_{\mathrm{NO_3+NH_4}}, N^{\mathrm{diat}}_{\mathrm{SiO_3}}\right)$$

Iron limitation of PFT *i*

$$N^i_{\mathrm{Fe}} = \frac{\mathrm{Fe}}{\mathrm{Fe} + K^i_{\mathrm{Fe}}}$$

Phosphate limitation of PFT *i*

$$N^i_{\mathrm{PO_4}} = \frac{\mathrm{PO_4}}{\mathrm{PO_4} + K^i_{\mathrm{PO_4}}}$$

Silicate limitation of diatoms

$$N^{\mathrm{diat}}_{\mathrm{SO_3}} = \frac{\mathrm{SO_3}}{\mathrm{SO_3} + K^{\mathrm{diat}}_{\mathrm{SO_3}}}$$

Nitrate and ammonium limitation of PFT *i*

$$N^{i}_{\mathrm{NO_3+NH_4}} = \frac{\mathrm{NO_3}}{K^{i}_{\mathrm{NO_3}} \cdot \left(1 + \frac{\mathrm{NO_3}}{K^{i}_{\mathrm{NO_3}}} + \frac{\mathrm{NH_4}}{K^{i}_{\mathrm{NH_4}}}\right)} + \frac{\mathrm{NH_4}}{K^{i}_{\mathrm{NH_4}} \cdot \left(1 + \frac{\mathrm{NO_3}}{K^{i}_{\mathrm{NO_3}}} + \frac{\mathrm{NH_4}}{K^{i}_{\mathrm{NH_4}}}\right)}$$

Light limitation of PFT *i*

$$L^{i}_{\mathrm{lim}} = 1 - e^{\frac{-\alpha^{i} \cdot \theta^{i}_{\mathrm{Chl/C}} \cdot I_{\mathrm{PAR}}}{\mu^{i}_{\mathrm{max}} \cdot T_{\mathrm{f}} \cdot N^{i}_{\mathrm{lim}}}}$$

Grazing

$$G_{\mathrm{nano}} = u^{\mathrm{nano}}_{\mathrm{max}} \cdot \mathrm{Tf} \cdot \frac{P^{2}_{\mathrm{nano}}}{P^{2}_{\mathrm{nano}} + g^{2}} \cdot Z$$

$$G_{\mathrm{diat}} = u^{\mathrm{diat}}_{\mathrm{max}} \cdot \mathrm{Tf} \cdot \frac{P^{2}_{\mathrm{diat}}}{P^{2}_{\mathrm{diat}} + g^{2} \cdot f^{\mathrm{diat}}_{z}} \cdot Z$$

A2 TOPAZ

Growth rate of phytoplankton PFT *i*

$$\mu^{i} = \frac{\mu^{i}_{\mathrm{max}}}{1.0 + \zeta} \cdot T_{\mathrm{f}} \cdot N^{i}_{\mathrm{lim}} \cdot L^{i}_{\mathrm{lim}}$$

Temperature function (for all PFTs)

$$T_\mathrm{f} = e^{k_\mathrm{Eppley} \cdot T}$$

Total nutrient limitation

$$N_\mathrm{lim}^\mathrm{nano} = \min\left(N_\mathrm{Fe}^\mathrm{nano}, N_{\mathrm{PO}_4}^\mathrm{nano}, N_{\mathrm{NO}_3+\mathrm{NH}_4}^\mathrm{nano}\right)$$

$$N_\mathrm{lim}^\mathrm{large} = \min\left(N_\mathrm{Fe}^\mathrm{large}, N_{\mathrm{PO}_4}^\mathrm{large}, N_{\mathrm{NO}_3+\mathrm{NH}_4}^\mathrm{large}\right)$$

The fraction of diatoms of large phytoplankton depends on the silicate concentration

$$P_\mathrm{Diatoms} = P_\mathrm{Large} \cdot N_{\mathrm{SO}_3}^\mathrm{diat}$$

Iron limitation of PFT *i*

$$N_\mathrm{Fe}^i = \frac{\left(Q_\mathrm{Fe/N}^i\right)^2}{\left(K_\mathrm{Fe/N}^i\right)^2 + \left(Q_\mathrm{Fe/N}^i\right)^2}, \text{ with } Q_\mathrm{Fe/N}^i = \min\left(Q_{(\mathrm{Fe/N,max})}^i, \theta_\mathrm{Fe/N}^i\right)$$

Phosphate limitation of PFT *i*

$$N_{\mathrm{PO}_4}^i = \frac{Q_\mathrm{P/N}^i}{Q_{(\mathrm{P/N,max})}^i}, \text{ with } Q_\mathrm{P/N}^i = \min\left(Q_{(\mathrm{P/N,max})}^i, \theta_\mathrm{P/N}^i\right)$$

Nitrate and ammonium limitation of PFT *i*

$$N_{\mathrm{NO}_3+\mathrm{NH}_4}^i = \frac{\mathrm{NO}_3}{\left(K_{\mathrm{NO}_3}^i + \mathrm{NO}_3\right)} \cdot \frac{1 + \mathrm{NH}_4}{K_{\mathrm{NH}_4}^i}$$

Silicate limitation of diatoms

$$N^{\mathrm{diat}}_{\mathrm{SO_3}} = \frac{\mathrm{SO_3}}{\mathrm{SO_3} + K^{\mathrm{diat}}_{\mathrm{SO_3}}}$$

Light limitation of PFT *i*

$$L^i_{\mathrm{lim}} = 1 - e^{\frac{-\alpha^i \cdot Q^i_{\mathrm{Chl/C}} \cdot I_{\mathrm{PAR}}}{\mu^i_{\mathrm{max}} \cdot T_{\mathrm{f}} \cdot N^i_{\mathrm{lim}}}}$$

$$\text{with } Q^i_{\mathrm{Chl/C}} = \frac{Q^i_{\mathrm{max}} - Q^i_{\mathrm{min}}}{1.0 + \left(Q^i_{\mathrm{max}} - Q^i_{\mathrm{min}}\right) \cdot \alpha^i v I_{\mathrm{Mem}} \cdot \frac{0.5}{\mu_{\mathrm{max}} \cdot N_{\mathrm{lim}} \cdot T_{\mathrm{f}}}} + Q^i_{\mathrm{min}}$$

$$\text{and } Q^i_{\mathrm{min}} = \max\left(0, Q^{\mathrm{nolim}}_{\mathrm{min}} - Q^{\mathrm{lim}}_{\mathrm{min}}\right) \cdot N^i_{\mathrm{lim}} \cdot Q^{\mathrm{lim}}_{\mathrm{min}}$$

I_{Mem} is the memory of irradiance over the scale of 24 h and was provided in the model output.

Grazing

$$G_{\mathrm{nano}} = \min\left(k_{\mathrm{graz_{max}}}, u_{\mathrm{max}} \cdot T_{\mathrm{f}} \cdot \frac{P_{\mathrm{nano}}}{P^\star}\right) \cdot \frac{P^2_{\mathrm{nano}}}{P_{\mathrm{nano}} + P_{\mathrm{min}}}$$

$$G_{\mathrm{large}} = \min\left(k_{\mathrm{graz_{max}}}, u_{\mathrm{max}} \cdot T_{\mathrm{f}} \cdot \left\{N^{\mathrm{graz}}_{\mathrm{large}}\right\}\right) \cdot P_{\mathrm{large}}$$

$$\left\{N^{\mathrm{graz}}_{\mathrm{large}}\right\} = \left[\frac{P_{\mathrm{large}} + P_{\mathrm{diaz}}}{P^\star}\right]^{\frac{1}{3}} \cdot \frac{P_{\mathrm{large}} + P_{\mathrm{diaz}}}{P_{\mathrm{large}} + P_{\mathrm{diaz}} + P_{\mathrm{min}}} \cdot \left(P^2_{\mathrm{large}} + P^2_{\mathrm{diaz}}\right)^{\frac{1}{2}}$$

Title Page
Abstract Introduction
Conclusions References
Tables Figures
◀| |▶
◀ ▶
Back Close
Full Screen / Esc
Printer-friendly Version
Interactive Discussion

A3 PISCES

Growth rate of phytoplankton PFT *i*

$$\mu^i = \mu_{\text{max}} \cdot T_\text{f} \cdot N^i_{\text{lim}} \cdot L^i_{\text{lim}}$$

Temperature function (for nanophytoplankton, diatoms and microzooplankton)

$$T_\text{f} = e^{k_{\text{Eppley}} \cdot T}$$

Temperature function (for mesozooplankton):

$$T_{f,\text{meso}} = e^{k_{\text{Eppley, meso}} \cdot T}$$

Total nutrient limitation

$$N^{\text{nano}}_{\text{lim}} = \min\left(N^{\text{nano}}_{\text{Fe}}, N^{\text{nano}}_{\text{PO}_4}, N^{\text{nano}}_{\text{NO}_3+\text{NH}_4}\right)$$

$$N^{\text{diat}}_{\text{lim}} = \min\left(N^{\text{diat}}_{\text{Fe}}, N^{\text{diat}}_{\text{PO}_4}, N^{\text{diat}}_{\text{NO}_3+\text{NH}_4}, N^{\text{diat}}_{\text{SiO}_3}\right)$$

Iron limitation of PFT *i*

$$N^i_{\text{Fe}} = \frac{\text{Fe}}{\text{Fe} + K^i_{\text{Fe, variable}}}$$

$$\text{where } K^i_{\text{Fe, variable}} = \max\begin{cases} K^i_{\text{Fe, min}} \\ \frac{\text{Diat}^* \cdot K^i_{\text{Fe, min}} + \text{Nano}^* \cdot K^i_{\text{Fe}}}{P_i} \end{cases}$$

$$\text{and Diat}^* = \min\begin{cases} P_{\text{diat}} \\ 5e^{-7} \end{cases} \text{ and Nano}^* = \min\begin{cases} P_{\text{nano}} \\ 1e^{-6} \end{cases}$$

Phosphate limitation of PFT *i*

$$N^i_{\mathrm{PO_4}} = \frac{\mathrm{PO_4}}{\mathrm{PO_4} + K^i_{\mathrm{PO_4}}}$$

Silicate limitation of diatoms

$$N^{\mathrm{diat}}_{\mathrm{SO_3}} = \frac{\mathrm{SO_3}}{\mathrm{SO_3} + K^{\mathrm{diat}}_{\mathrm{SO_3}}}$$

Nitrate and ammonium limitation of PFT *i*

$$N^i_{\mathrm{NO_3+NH_4}} = \frac{K^i_{\mathrm{NH_4}} \cdot \mathrm{NO_3} + K^i_{\mathrm{NO_3}} \cdot \mathrm{NH_4}}{K^i_{\mathrm{NH_4}} K^i_{\mathrm{NO_3}} + K^i_{\mathrm{NH_4}} \mathrm{NO_3} + K^i_{\mathrm{NO_3}} \mathrm{NH_4}}$$

Light limitation of PFT *i*

$$L^i_{\mathrm{lim}} = \left(1 - \frac{\{\mathrm{MXL\ influence}\}}{\beta_i + \{\mathrm{MXL\ influence}\}}\right) \cdot \left(1 - e^{\frac{-\alpha \cdot \theta^i_{\mathrm{Chl/C}} \cdot I_{\mathrm{PAR}}}{\mu^i_{\mathrm{max}} \cdot N^i_{\mathrm{lim}}}}\right)$$

$$\text{with } \{\mathrm{MXL\ influence}\} = \begin{cases} \mathrm{MXL} - \mathrm{Heup} & \text{if} \quad \mathrm{MXL} > \mathrm{Heup} \\ 0 & \text{otherwise} \end{cases}$$

where MXL denotes the mixed layer depth and Heup the depth of the euphotic zone.

Microzooplankton grazing

$$G_{\mathrm{micro \to nano}} = u^{\mathrm{micro \to nano}}_{\mathrm{max}} \cdot T_{\mathrm{f}} \cdot \frac{\Psi^{\mathrm{micro}}_{\mathrm{nano}} P_{\mathrm{nano}}}{\sum_l \Psi^{\mathrm{micro}}_{\mathrm{nano}} \cdot l} \cdot \frac{P_{\mathrm{nano}}}{K_{\mathrm{G}} + \sum_l \left(\Psi^{\mathrm{micro}}_l \cdot l\right)}$$

l denotes the food options and consists of diatoms and nanophytoplankton for microzooplankton. Grazing on diatoms is calculated accordingly.

Mesozooplankton grazing

$$G_{\text{meso}\to\text{nano}} = u_{\max}^{\text{meso}\to\text{nano}} \cdot T_{f,\text{meso}} \cdot \frac{\Psi_{\text{nano}}^{\text{meso}} P_{\text{nano}}}{K^G + \sum_l \Psi_{\text{nano}}^{\text{meso}} \cdot l} \cdot Z_{\text{meso}}$$

The food options l for mesozooplankton are nanophytoplankton, diatoms and microzooplankton.

A4 MEM

Growth rate of phytoplankton PFT *i*

$$\mu^i = \mu_{\max}^i \cdot T_{\text{f}} \cdot N_{\text{lim}}^i \cdot L_{\text{lim}}^i$$

Temperature function (for all PFTs)

$$T_{\text{f}} = e^{k_{\text{Eppley}} \cdot T}$$

Total nutrient limitation

$$N_{\text{lim}}^{\text{nano}} = \min\left(N_{\text{Fe}}^{\text{nano}}, N_{\text{NO}_3+\text{NH}_4}^{\text{nano}}\right)$$

$$N_{\text{lim}}^{\text{diat}} = \min\left(N_{\text{Fe}}^{\text{diat}}, N_{\text{NO}_3+\text{NH}_4}^{\text{diat}}, N_{\text{SiO}_3}^{\text{diat}}\right)$$

Iron limitation of PFT *i*

$$N^i_{\mathrm{Fe}} = \frac{\mathrm{Fe}}{\frac{\mathrm{Fe}}{1-f^i_{\mathrm{A}}} + \frac{\mu^i_{\max}}{f^i_{\mathrm{A}} A^i_{\mathrm{Fe}}}}$$

$$\text{with } f^i_{\mathrm{A}} = \max\left\{ \begin{array}{l} \left(1+\sqrt{\frac{\max(A^i_{\mathrm{NO_3}}\cdot \mathrm{NO_3}, A^i_{\mathrm{NH_4}}\cdot \mathrm{NH_4})}{\mu^i_{\max}}}\right)^{-1} \\ \left(1+\sqrt{\frac{A^i_{\mathrm{Fe}}\cdot \mathrm{Fe}}{\mu^i_{\max}}}\right)^{-1} \end{array} \right.$$

Silicate limitation of diatoms

$$N^{\mathrm{diat}}_{\mathrm{SO_3}} = \frac{\mathrm{SO_3}}{\frac{\mathrm{SO_3}}{1-f^{\mathrm{diat}}_{A}} + \frac{\mu^{\mathrm{diat}}_{\mathrm{mac}}}{f^{\mathrm{diat}}_{A}\cdot A^{\mathrm{diat}}_{\mathrm{Si}}}}$$

Nitrate and ammonium limitation of PFT *i*

$$N^i_{\mathrm{NO_3+NH_4}} = \frac{\mathrm{NO_3}}{\frac{\mathrm{NO_3}}{1-f^i_{\mathrm{A}}} + \frac{\mu^i_{\max}}{f^i_{\mathrm{A}}\cdot A^i_{\mathrm{NO_3}}}} \left(1 - \frac{\mathrm{NH_4}}{\mathrm{NH_4} + K^i_{\mathrm{NH_4}}}\right) + \frac{\mathrm{NH_4}}{\frac{\mathrm{NH_4}}{1-f^i_{\mathrm{A}}} + \frac{\mu^i_{\max}}{f^i_{\mathrm{A}}\cdot A^i_{\mathrm{NH_4}}}}$$

Light limitation of PFT *i*

$$L_{\mathrm{lim}} = \frac{\left(1 - e^{\left(-\frac{\alpha_i\cdot \mathrm{PAR}}{p_{\mathrm{r}}}\right)}\right)\cdot e^{\frac{\beta\cdot \mathrm{PAR}}{p^i_S}}}{\frac{\alpha_i}{\alpha_i+\beta}\cdot \frac{\beta}{\alpha_i+\beta_i}^{\frac{\beta}{\alpha_i}}}$$

Title Page
Abstract
Introduction
Conclusions
References
Tables
Figures
◀▶
Back
Close
Full Screen / Esc
Printer-friendly Version
Interactive Discussion

Grazing

$$G_{\text{micro}\to\text{nano}} = u_{\text{max}}^{\text{micro}\to\text{nano}} \cdot T_{\text{f}} \cdot Z_{\text{micro}} \cdot \max\begin{cases}0\\ 1-e^{\lambda\left(T_{\text{nano}}^{\text{micro}}-P_{\text{nano}}\right)}\end{cases}$$

$G_{\text{meso}\to\text{nano}}, G_{\text{meso}\to\text{diat}}, G_{\text{meso}\to\text{micro}}, G_{\text{pred}\to\text{diat}}$ are all calculated using the same equation but different parameters.

$$G_{\text{pred}\to\text{micro}} = u_{\text{max}}^{\text{pred}\to\text{micro}} \cdot T_{\text{f}} \cdot Z_{\text{pred}} \cdot \max\begin{cases}0\\ 1-e^{\lambda\left(T_{\text{micro}}^{\text{pred}}-P_{\text{micro}}\right)}\end{cases} \cdot e^{-\Psi_{\text{micro}} Z_{\text{pred}}}$$

$G_{\text{pred}\to\text{meso}}$ analog.

A5 PELAGOS

Growth rate of phytoplankton PFT *i*

$$\mu^i = \mu_{\text{max}}^i \cdot T_{\text{f}} \cdot \left\{N_{\text{lim, Fe}}^i \cdot N_{\text{lim, Si}}^i\right\} \cdot L_{\text{lim}}^i$$

Nutrient limitation with respect to phosphate and nitrate is not included in the phytoplankton growth rate, but acts through the exudation and lysis terms. The exudation and lysis terms have not been recalculated in this work, instead we estimated a multiplicative nutrient limitation factor (see Sect. 1). We refer to Vichi et al. (2007) for a full description of the nutrient limitation in PELAGOS.

Temperature function for PFT *i*

$$T_{\text{f}} = \left(Q_{10}^i\right)^{\frac{T-10}{10}}$$

Light limitation of PFT *i*

$$L^{i}_{\text{lim}} = 1 - e^{\frac{-\alpha^{i}\cdot\theta^{i}_{\text{Chl/C}}\cdot I_{\text{PAR}}}{\mu^{i}_{\text{max}}}}$$

Grazing

Grazing of zooplankton type i on phytoplankton type j is calculated as:

$$G^{i\rightarrow j} = u^{i}_{\text{max}}\cdot \text{Tf}\cdot \frac{\delta^{i}_{j}\cdot e^{i}_{j}\cdot P_{j}}{F}\cdot \frac{F}{F + K^{F}_{1/2}}\cdot Z_{i}$$

where F denotes the total food available and is calculated as:

$$F = \sum_{j}\delta^{i}_{j}\cdot e^{i}_{j}\cdot P_{j}$$

e^{i}_{j} denotes the capture efficiency of zooplankton i when grazing on phytoplankton j, and is set so 1.0 for mesozooplankton, but depends on prey density for microzooplankton and heterotrophic flagellates:

$$e^{\text{micro, flagellates}}_{j} = \frac{P_{j}}{P_{j} + \mu_{\text{micro, flagellates}}}$$

A6 PlankTOM5.3

Growth rate of phytoplankton PFT *i*

$$\mu^{i} = \mu^{i}_{\text{max}}\cdot T_{\text{f}}\cdot N^{i}_{\text{lim}}\cdot L^{i}_{\text{lim}}$$

Title Page

Abstract Introduction

Conclusions References

Tables Figures

◄◄ ►►

◄ ►

Back Close

Full Screen / Esc

Printer-friendly Version

Interactive Discussion

Temperature function for PFT *i*

$$T_\mathrm{f} = \left(Q^i_{10}\right)^{\frac{T}{10}}$$

Total nutrient limitation

$$N^\mathrm{nano}_\mathrm{lim} = \min\left(N^\mathrm{nano}_\mathrm{Fe}, N^\mathrm{nano}_{\mathrm{NO}_3}\right)$$

$$N^\mathrm{diat}_\mathrm{lim} = \min\left(N^\mathrm{diat}_\mathrm{Fe}, N^\mathrm{diat}_{\mathrm{NO}_3}, N^\mathrm{diat}_{\mathrm{SiO}_3}\right)$$

Iron limitation of PFT *i*

$$N^i_\mathrm{Fe} = \frac{\theta^i_\mathrm{Fe/C} - \theta^i_\mathrm{Fe/C,min}}{\theta^i_\mathrm{Fe/C,opt} - \theta^i_\mathrm{Fe/C,min}}$$

Silicate limitation of diatoms

$$N^\mathrm{diat}_{\mathrm{SO}_3} = \frac{\mathrm{SO}_3}{\mathrm{SO}_3 + K^\mathrm{diat}_{\mathrm{SO}_3}}$$

Nitrate and ammonium limitation of PFT *i*

$$N^i_{\mathrm{NO}_3} = \frac{\mathrm{NO}_3}{\mathrm{NO}_3 + K^i_{\mathrm{NO}_3}}$$

Light limitation of PFT *i*

$$L^i_\mathrm{lim} = 1 - e^{\frac{-\alpha^i \cdot \theta^i_\mathrm{Chl/C} \cdot I_\mathrm{PAR}}{\mu^i_\mathrm{max} \cdot T_\mathrm{f} \cdot N^i_\mathrm{lim}}}$$

Title Page
Abstract Introduction
Conclusions References
Tables Figures
◀I ▶I
◀ ▶
Back Close
Full Screen / Esc
Printer-friendly Version
Interactive Discussion

Grazing

$$G_{\text{micro}} = u_{\text{max}}^{\text{micro}} \cdot T_{\text{f}} \cdot \frac{\Psi^{i}_{\text{micro}} P_i}{K_{1/2}^{\text{micro}} + \sum_{i \in F} \Psi^{i}_{\text{micro}} P_i} \cdot Z_{\text{micro}}$$

The food sources F for microzooplankton are small phytoplankton, diatoms, coccolithophores and small particulate organic carbon.

$$G_{\text{meso}} = u_{\text{max}}^{\text{meso}} \cdot T_{\text{f, meso}} \cdot \frac{\Psi^{i}_{\text{meso}} P_i}{K_{1/2}^{\text{meso}} + \sum_{i \in F} \Psi^{i}_{\text{meso}} P_i} \cdot Z_{\text{meso}}$$

The food sources F for mesozooplankton are small phytoplankton, diatoms, coccolithophores and small particulate organic carbon.

A7 REcoM2

Growth rate of phytoplankton PFT *i*

$$\mu^i = \mu^i_{\text{max}} \cdot T_{\text{f}} \cdot N^i_{\text{lim}} \cdot L^i_{\text{lim}}$$

Temperature function for all PFTs

$$T_{\text{f}} = e^{-4500 \cdot \left(\frac{1}{T} - \frac{1}{T_{\text{ref}}}\right)}$$

Total nutrient limitation

$$N^{\text{nano}}_{\text{lim}} = \min\left(N^{\text{nano}}_{\text{Fe}}, N^{\text{nano}}_{\text{N}}\right)$$

$$N^{\text{diat}}_{\text{lim}} = \min\left(N^{\text{diat}}_{\text{Fe}}, N^{\text{diat}}_{\text{N}}, N^{\text{diat}}_{\text{SiO}_3}\right)$$

Iron limitation of PFT i

$$N_{\mathrm{Fe}}^{i} = \frac{\mathrm{Fe}}{\mathrm{Fe} + K_{\mathrm{Fe}}^{i}}$$

Silicate limitation of diatoms

$$N_{\mathrm{SO_3}}^{\mathrm{diat}} = \begin{cases} 1 - e^{\left(-4\theta_{\mathrm{min}}^{\mathrm{SiO_3}}\left(\theta_{\mathrm{Si/C,min}} - \theta_{\mathrm{Si/C}}^{\mathrm{diat}}\right)^2\right)} & \theta_{\mathrm{Si/C,min}} < \theta_{\mathrm{Si/C}}^{\mathrm{diat}} \\ 0 & \theta_{\mathrm{Si/C,min}} \geq \theta_{\mathrm{Si/C}}^{\mathrm{diat}} \end{cases}$$

Nitrate and ammonium limitation of PFT i

$$N_{\mathrm{N}}^{i} = \begin{cases} 1 - e^{\left(-4\theta_{\mathrm{min}}^{N}\left(\theta_{\mathrm{N/C,min}} - \theta_{\mathrm{N/C}}^{i}\right)^2\right)} & \theta_{\mathrm{N/C,min}} < \theta_{\mathrm{N/C}}^{i} \\ 0 & \theta_{\mathrm{N/C,min}} \geq \theta_{\mathrm{N/C}}^{i} \end{cases}$$

Light limitation of PFT i

$$L_{\mathrm{lim}}^{i} = 1 - e^{\frac{-\alpha^{i}\cdot\theta_{\mathrm{Chl/C}}^{i}\cdot I_{\mathrm{PAR}}}{\mu_{\mathrm{max}}^{i}\cdot T_{\mathrm{f}}\cdot N_{\mathrm{lim}}^{i}}}$$

Grazing

$$G_{\mathrm{nano}} = u_{\mathrm{max}} \cdot T_{\mathrm{f}} \cdot \frac{(P_{\mathrm{nano}} + \Psi_{\mathrm{diat}} P_{\mathrm{diat}})}{K_{\mathrm{zoo}} + (P_{\mathrm{nano}} + \Psi_{\mathrm{diat}} P_{\mathrm{diat}})^2} \cdot P_{\mathrm{nano}} \cdot Z$$

$$G_{\mathrm{diat}} = u_{\mathrm{max}} \cdot T_{\mathrm{f}} \cdot \frac{(P_{\mathrm{nano}} + \Psi_{\mathrm{diat}} P_{\mathrm{diat}})}{K_{\mathrm{zoo}} + (P_{\mathrm{nano}} + \Psi_{\mathrm{diat}} P_{\mathrm{diat}})^2} \cdot \Psi_{\mathrm{diat}} P_{\mathrm{diat}} \cdot Z$$

Acknowledgements. CL and the research leading to these results have received funding from the European Community's Seventh Framework Programme (FP7 2007-2013) under grant agreements n 238366 (Greencycles II) and 264879 (CarboChange). MV and NG acknowledge funding by ETH Zürich. SCD and IDL acknowledge support from NSF (AGS-1048827). We thank the climate modeling groups for calculating and providing their model output. We also acknowledge the World Climate Research Programme's Working Group on Coupled Modelling, which is responsible for CMIP. For CMIP the US Department of Energy's Program for Climate Model Diagnosis and Intercomparison provided coordinating support and led the development of software infrastructure in partnership with the Global Organization for Earth System Science Portals. We thank T. Frölicher and C. O'Brien for fruitful discussions. This is a contribution from the MAREMIP project.

References

Allen, M. R. and Ingram, W. J.: Constraints on future changes in climate and the hydrologic cycle, Nature, 419, 224–232, doi:10.1038/nature01092, 2002. 3765

Alvain, S., Le Quéré, C., Bopp, L., Racault, M.-F., Beaugrand, G., Dessailly, D., and Buitenhuis, E. T.: Rapid climatic driven shifts of diatoms at high latitudes, Remote Sens. Environ., 132, 195–201, doi:10.1016/j.rse.2013.01.014, 2013. 3736

Antoine, D., Morel, A., Gordon, H. R., Banzon, V. F., and Evans, R. H.: Bridging ocean color observations of the 1980s and 2000s in search of long-term trends, J. Geophys. Res., 110, C06009, doi:10.1029/2004JC002620, 2005. 3735

Aumont, O. and Bopp, L.: Globalizing results from ocean in situ iron fertilization studies, Global Biogeochem. Cy., 20, 1–15, doi:10.1029/2005GB002591, 2006. 3796

Behrenfeld, M. J.: Abandoning Sverdrup's Critical Depth Hypothesis on phytoplankton blooms, Ecology, 91, 977–989, 2010. 3736

Behrenfeld, M. J. and Falkowski, P. G.: Photosynthetic rates derived from satellite-based chlorophyll concentration, Limnol. Oceanogr., 42, 1–20, 1997. 3824

Behrenfeld, M. J., O'Malley, R. T., Siegel, D. A., McClain, C. R., Sarmiento, J. L., Feldman, G. C., Milligan, A. J., Falkowski, P. G., Letelier, R. M., and Boss, E. S.: Climate-driven trends in contemporary ocean productivity, Nature, 444, 752–755, doi:10.1038/nature05317, 2006. 3735

Behrenfeld, M. J., Doney, S. C., Lima, I., Boss, E. S., and Siegel, D. A.: Annual cycles of ecological disturbance and recovery underlying the subarctic Atlantic spring plankton bloom, Global Biogeochem. Cy., 27, 526–540, doi:10.1002/gbc.20050, 2013. 3736

Bopp, L., Monfray, P., Aumont, O., Dufresne, J., Le Treut, H., Madec, G., Terray, L., and Orr, J.: Potential impact of climate change on marine export production, Global Biogeochem. Cy., 15, 81–100, 2001. 3734, 3735, 3736, 3758, 3760

Bopp, L., Aumont, O., Cadule, P., Alvain, S., and Gehlen, M.: Response of diatoms distribution to global warming and potential implications: a global model study, Geophys. Res. Lett., 32, 2–5, doi:10.1029/2005GL023653, 2005. 3736, 3761, 3762

Bopp, L., Resplandy, L., Orr, J. C., Doney, S. C., Dunne, J. P., Gehlen, M., Halloran, P., Heinze, C., Ilyina, T., Séférian, R., Tjiputra, J., and Vichi, M.: Multiple stressors of ocean ecosystems in the 21st century: projections with CMIP5 models, Biogeosciences, 10, 6225–6245, doi:10.5194/bg-10-6225-2013, 2013. 3734, 3736, 3745, 3746, 3763, 3797

Boyce, D. G., Lewis, M. R., and Worm, B.: Global phytoplankton decline over the past century, Nature, 466, 591–596, doi:10.1038/nature09268, 2010. 3735

Boyd, P. W. and Doney, S. C.: Modelling regional responses by marine pelagic ecosystems to global climate change, Geophys. Res. Lett., 29, 1–4, doi:10.1029/2001GL014130, 2002. 3734

Buitenhuis, E. T., Hashioka, T., and Le Quéré, C.: Combined constraints on global ocean primary production using observations and models, Global Biogeochem. Cy., 27, 847–858, doi:10.1002/gbc.20074, 2013a. 3745, 3796

Buitenhuis, E. T., Vogt, M., Moriarty, R., Bednaršek, N., Doney, S. C., Leblanc, K., Le Quéré, C., Luo, Y.-W., O'Brien, C., O'Brien, T., Peloquin, J., Schiebel, R., and Swan, C.: MAREDAT: towards a world atlas of MARine Ecosystem DATa, Earth Syst. Sci. Data, 5, 227–239, doi:10.5194/essd-5-227-2013, 2013b. 3766

Cagnazzo, C., Manzini, E., Fogli, P. G., Vichi, M., and Davini, P.: Role of stratospheric dynamics in the ozone–carbon connection in the Southern Hemisphere, Clim. Dynam., 41, 3039–3054, 2013. 3796

Carr, M., Friedrichs, M., Schmeltz, M., Noguchiaita, M., Antoine, D., Arrigo, K., Asanuma, I., Aumont, O., Barber, R., and Behrenfeld, M.: A comparison of global estimates of marine primary production from ocean color, Deep-Sea Res. Pt. II, 53, 741–770, doi:10.1016/j.dsr2.2006.01.028, 2006. 3745, 3824

Collins, W. J., Bellouin, N., Doutriaux-Boucher, M., Gedney, N., Halloran, P., Hinton, T., Hughes, J., Jones, C. D., Joshi, M., Liddicoat, S., Martin, G., O'Connor, F., Rae, J., Senior, C., Sitch, S., Totterdell, I., Wiltshire, A., and Woodward, S.: Development and evaluation of an Earth-System model – HadGEM2, Geosci. Model Dev., 4, 1051–1075, doi:10.5194/gmd-4-1051-2011, 2011. 3796

Doney, S. C., Fabry, V. J., Feely, R. A., and Kleypas, J. A.: Ocean acidification: the other CO_2 problem, Annual Review of Marine Science, 1, 169–192, doi:10.1146/annurev.marine.010908.163834, 2009. 3768

Duarte, C. M., Regaudie-de Gioux, A., Arrieta, J. M., Delgado-Huertas, A., and Agustí, S.: The oligotrophic ocean is heterotrophic, Annual Review of Marine Science, 5, 551–569, doi:10.1146/annurev-marine-121211-172337, 2013. 3770

Ducklow, H. W. and Doney, S. C.: What is the metabolic state of the oligotrophic ocean? A debate, Annual Review of Marine Science, 5, 525–533, doi:10.1146/annurev-marine-121211-172331, 2013. 3770

Dufresne, J.-L., Foujols, M.-A., Denvil, S., Caubel, A., Marti, O., Aumont, O., Balkanski, Y., Bekki, S., Bellenger, H., Benshila, R., Bony, S., Bopp, L., Braconnot, P., Brockmann, P., Cadule, P., Cheruy, F., Codron, F., Cozic, A., Cugnet, D., Noblet, N., Duvel, J.-P., Ethé, C., Fairhead, L., Fichefet, T., Flavoni, S., Friedlingstein, P., Grandpeix, J.-Y., Guez, L., Guilyardi, E., Hauglustaine, D., Hourdin, F., Idelkadi, A., Ghattas, J., Joussaume, S., Kageyama, M., Krinner, G., Labetoulle, S., Lahellec, A., Lefebvre, M.-P., Lefevre, F., Levy, C., Li, Z. X., Lloyd, J., Lott, F., Madec, G., Mancip, M., Marchand, M., Masson, S., Meurdesoif, Y., Mignot, J., Musat, I., Parouty, S., Polcher, J., Rio, C., Schulz, M., Swingedouw, D., Szopa, S., Talandier, C., Terray, P., Viovy, N., and Vuichard, N.: Climate change projections using the IPSL-CM5 Earth System Model: from CMIP3 to CMIP5, Clim. Dynam., 40, 2123–2165, doi:10.1007/s00382-012-1636-1, 2013. 3796

Dunne, J. P., Armstrong, R. A., Gnanadesikan, A., and Sarmiento, J. L.: Empirical and mechanistic models for the particle export ratio, Global Biogeochem. Cy., 19, 1–16, doi:10.1029/2004GB002390, 2005. 3742

Dunne, J. P., Hales, B., and Toggweiler, J. R.: Global calcite cycling constrained by sediment preservation controls, Global Biogeochem. Cy., 26, GB3023, doi:10.1029/2010GB003935, 2012. 3796

Dunne, J. P., John, J. G., Shevliakova, E., Stouffer, R. J., Krasting, J. P., Malyshev, S. L., Milly, P. C. D., Sentman, L. T., Adcroft, A. J., Cooke, W., Dunne, K. A., Griffies, S. M., Hallberg, R. W., Harrison, M. J., Levy, H., Wittenberg, A. T., Phillips, P. J., and Zadeh, N.: GFDL's ESM2 global coupled climate–carbon Earth system models. Part II: Carbon system formulation and baseline simulation characteristics*, J. Climate, 26, 2247–2267, doi:10.1175/JCLI-D-12-00150.1, 2013. 3796

Dutkiewicz, S., Scott, J. R., and Follows, M. J.: Winners and losers: ecological and biogeochemical changes in a warming ocean, Global Biogeochem. Cy., 27, 463–477, doi:10.1002/gbc.20042, 2013. 3736, 3760, 3761

Edwards, A. M. and Yool, A.: The role of higher predation in plankton population models, J. Plankton Res., 22, 1085–1112, 2000. 3771

Eppley, R.: Temperature and phytoplankton growth in the sea, Fishery Bulletin, 70, 1063–1085, 1972. 3740

Falkowski, P. G., Laws, E. A., Barber, R. T., and Murray, J. W.: Phytoplankton and their role in primary, new, and export production, in: Ocean Biogeochemistry: the Role of the Ocean Carbon Cycle in Global Change, edited by: Fasham, M. J. R., The IGBP Series, Springer, Berlin, chap. 4, 99–121, 2003. 3734

Finkel, Z. V., Beardall, J., Flynn, K. J., Quigg, A., Rees, T. A. V., and Raven, J. A.: Phytoplankton in a changing world: cell size and elemental stoichiometry, J. Plankton Res., 32, 119–137, doi:10.1093/plankt/fbp098, 2009. 3768

Garcia, H. E., Locarnini, R. A., Boyer, T. P., Antonov, J. I., Baranova, O. K., Zweng, M. M., Reagan, J. R., and Johnson, D. R.: World Ocean Atlas 2013, Volume 4: Dissolved Inorganic Nutrients (phosphate, nitrate, silicate), edited by: Levitus, S., and Mishonov, A., NOAA Atlas NESDIS 76, 25 pp., 2014. 3744, 3803

García-Corral, L. S., Barber, E., Regaudie-de-Gioux, A., Sal, S., Holding, J. M., Agustí, S., Navarro, N., Serret, P., Mozetič, P., and Duarte, C. M.: Temperature dependence of planktonic metabolism in the subtropical North Atlantic Ocean, Biogeosciences, 11, 4529–4540, doi:10.5194/bg-11-4529-2014, 2014. 3770

Geider, R. J., MacIntyre, H. L., and Kana, T. M.: A dynamic regulatory model of phytoplanktonic acclimation to light, nutrients, and temperature, Limnol. Oceanogr., 43, 679–694, doi:10.4319/lo.1998.43.4.0679, 1998. 3741

Gregg, W. W.: Ocean primary production and climate: global decadal changes, Geophys. Res. Lett., 30, 10–13, doi:10.1029/2003GL016889, 2003. 3735

Hancke, K. and Glud, R.: Temperature effects on respiration and photosynthesis in three diatom-dominated benthic communities, Aquat. Microb. Ecol., 37, 265–281, doi:10.3354/ame037265, 2004. 3770

Hashioka, T., Vogt, M., Yamanaka, Y., Le Quéré, C., Buitenhuis, E. T., Aita, M. N., Alvain, S., Bopp, L., Hirata, T., Lima, I., Sailley, S., and Doney, S. C.: Phytoplankton competition during the spring bloom in four plankton functional type models, Biogeosciences, 10, 6833–6850, doi:10.5194/bg-10-6833-2013, 2013. 3736, 3738, 3766

Hauck, J., Völker, C., Wang, T., Hoppema, M., Losch, M., and Wolf-Gladrow, D. A.: Seasonally different carbon flux changes in the Southern Ocean in response to the southern annular mode, Global Biogeochem. Cy., 27, 1236–1245, doi:10.1002/2013GB004600, 2013. 3796

Henson, S. A., Sanders, R., Madsen, E., Morris, P. J., Le Moigne, F., and Quartly, G. D.: A reduced estimate of the strength of the ocean's biological carbon pump, Geophys. Res. Lett., 38, L04606, doi:10.1029/2011GL046735, 2011. 3735

Hirst, A. G. and Bunker, A. J.: Growth of marine planktonic copepods: global rates and patterns in relation to chlorophyll *a*, temperature, and body weight, Limnol. Oceanogr., 48, 1988–2010, doi:10.4319/lo.2003.48.5.1988, 2003. 3770

Hurrell, J. W., Holland, M. M., Gent, P. R., Ghan, S., Kay, J. E., Kushner, P. J., Lamarque, J.-F., Large, W. G., Lawrence, D., Lindsay, K., Lipscomb, W. H., Long, M. C., Mahowald, N., Marsh, D. R., Neale, R. B., Rasch, P., Vavrus, S., Vertenstein, M., Bader, D., Collins, W. D., Hack, J. J., Kiehl, J., and Marshall, S.: The Community Earth System Model: a framework for collaborative research, B. Am. Meteorol. Soc., 94, 1339–1360, doi:10.1175/BAMS-D-12-00121.1, 2013. 3796

Ikeda, T., Kanno, Y., Ozaki, K., and Shinada, A.: Metabolic rates of epipelagic marine copepods as a function of body mass and temperature, Mar. Biol., 139, 587–596, doi:10.1007/s002270100608, 2001. 3770

Kwiatkowski, L., Yool, A., Allen, J. I., Anderson, T. R., Barciela, R., Buitenhuis, E. T., Butenschön, M., Enright, C., Halloran, P. R., Le Quéré, C., de Mora, L., Racault, M.-F., Sinha, B., Totterdell, I. J., and Cox, P. M.: iMarNet: an ocean biogeochemistry model intercomparison project within a common physical ocean modelling framework, Biogeosciences, 11, 7291–7304, doi:10.5194/bg-11-7291-2014, 2014. 3763

Laufkötter, C., Vogt, M., and Gruber, N.: Long-term trends in ocean plankton production and particle export between 1960–2006, Biogeosciences, 10, 7373–7393, doi:10.5194/bg-10-7373-2013, 2013. 3735

Le Quéré, C., Harrison, S. P., Prentice, I., Buitenhuis, E. T., Aumont, O., Bopp, L., Claustre, H., Da Cunha, L. C., Geider, R., Giraud, X., Klaas, C., Kohfeld, K. E., Legendre, L., Manizza, M., Platt, T., Rivkin, R. B., Sathyendranath, S., Uitz, J., Watson, A. J., and Wolf-Gladrow, D.: Ecosystem dynamics based on plankton functional types for global ocean biogeochemistry models, Glob. Change Biol., 11, 2016–2040, doi:10.1111/j.1365-2486.2005.1004.x, 2005. 3735

Levitan, O., Rosenberg, G., Setlik, I., Setlikova, E., Grigel, J., Klepetar, J., Prasil, O., and Berman-Frank, I.: Elevated CO_2 enhances nitrogen fixation and growth in the marine cyanobacterium *Trichodesmium*, Glob. Change Biol., 13, 531–538, doi:10.1111/j.1365-2486.2006.01314.x, 2007. 3768

Liebig, J.: Chemistry and its Applications to Agriculture and Physiology: on Chemical Processes in the Nutrition of Vegetables, Taylor and Walton, London, 1840. 3740

Lindsay, K., Bonan, G. B., Doney, S. C., Hoffman, F. M., Lawrence, D. M., Long, M. C., Mahowald, N. M., Moore, J. K., Randerson, J. T., and Thornton, P. E.: Preindustrial control and 20th century carbon cycle experiments with the Earth system model CESM1(BGC), J. Climate, 1, 8981–9005, doi:10.1175/JCLI-D-12-00565.1, 2014. 3796

Lomas, M. W., Glibert, P. M., Shiah, F.-K., and Smith, E. M.: Microbial processes and temperature in Chesapeake Bay: current relationships and potential impacts of regional warming, Glob. Change Biol., 8, 51–70, doi:10.1046/j.1365-2486.2002.00454.x, 2002. 3770

López-Urrutia, A., San Martin, E., Harris, R. P., and Irigoien, X.: Scaling the metabolic balance of the oceans, P. Natl. Acad. Sci. USA, 103, 8739–8744, doi:10.1073/pnas.0601137103, 2006. 3770

Mahlstein, I., Gent, P. R., and Solomon, S.: Historical Antarctic mean sea ice area, sea ice trends, and winds in CMIP5 simulations, J. Geophys. Res.-Atmos., 118, 5105–5110, doi:10.1002/jgrd.50443, 2013. 3748

Manizza, M., Buitenhuis, E. T., and Le Quéré, C.: Sensitivity of global ocean biogeochemical dynamics to ecosystem structure in a future climate, Geophys. Res. Lett., 37, 3–7, doi:10.1029/2010GL043360, 2010. 3761

Marinov, I., Doney, S. C., and Lima, I. D.: Response of ocean phytoplankton community structure to climate change over the 21st century: partitioning the effects of nutrients, temperature and light, Biogeosciences, 7, 3941–3959, doi:10.5194/bg-7-3941-2010, 2010. 3736, 3758, 3761, 3762

Marinov, I., Doney, S. C., Lima, I. D., Lindsay, K., Moore, J. K., and Mahowald, N.: North–South asymmetry in the modeled phytoplankton community response to climate change over the 21st century, Global Biogeochem. Cy., 27, GB004599, doi:10.1002/2013GB004599, 2013. 3734, 3736, 3759, 3761, 3762

Michaelis, L. and Menten, M.: Die Kinetik der Invertinwirkung, Biochem. Z., 49, 333–369, 1913. 3740

Moore, J., Doney, S., Kleypas, J., Glover, D., and Fung, I.: An intermediate complexity marine ecosystem model for the global domain, Deep-Sea Res. Pt. II, 49, 403–462, doi:10.1016/S0967-0645(01)00108-4, 2002. 3758

Moore, C. M., Mills, M. M., Arrigo, K. R., Berman-Frank, I., Bopp, L., Boyd, P. W., Galbraith, E. D., Geider, R. J., Guieu, C., Jaccard, S. L., Jickells, T. D., La Roche, J., Lenton, T. M., Mahowald, N. M., Marañón, E., Marinov, I., Moore, J. K., Nakatsuka, T., Oschlies, A., Saito, M. A., Thingstad, T. F., Tsuda, A., and Ulloa, O.: Processes and patterns of oceanic nutrient limitation, Nat. Geosci., 6, 701–710, doi:10.1038/ngeo1765, 2013a. 3749, 3764

Moore, J. K., Lindsay, K., Doney, S. C., Long, M. C., and Misumi, K.: Marine ecosystem dynamics and biogeochemical cycling in the Community Earth System Model [CESM1(BGC)]: comparison of the 1990s with the 2090s under the RCP4.5 and RCP8.5 scenarios, J. Climate, 26, 9291–9312, doi:10.1175/JCLI-D-12-00566.1, 2013b. 3796

Morán, X. A. G., López-Urrutia, A., Calvo-Díaz, A., and Li, W. K. W.: Increasing importance of small phytoplankton in a warmer ocean, Glob. Change Biol., 16, 1137–1144, 2010. 3736

Platt, T., Gallegos, C., and Harrison, W.: Photoinhibition of photosynthesis in natural assemblages of marine phytoplankton in the Arctic, Deep-Sea Res., 29, 1159–1170, 1980. 3741

Prowe, A. E. F., Pahlow, M., Dutkiewicz, S., Follows, M., and Oschlies, A.: Top-down control of marine phytoplankton diversity in a global ecosystem model, Prog. Oceanogr., 101, 1–13, doi:10.1016/j.pocean.2011.11.016, 2011. 3736, 3768

Prowe, A. E. F., Pahlow, M., and Oschlies, A.: Controls on the diversity–productivity relationship in a marine ecosystem model, Ecol. Model., 225, 167–176, doi:10.1016/j.ecolmodel.2011.11.018, 2012. 3736, 3768

Prowe, A. E. F., Pahlow, M., Dutkiewicz, S., and Oschlies, A.: How important is diversity for capturing environmental-change responses in ecosystem models?, Biogeosciences, 11, 3397–3407, doi:10.5194/bg-11-3397-2014, 2014. 3768

Ridgwell, A., Schmidt, D. N., Turley, C., Brownlee, C., Maldonado, M. T., Tortell, P., and Young, J. R.: From laboratory manipulations to Earth system models: scaling calcification impacts of ocean acidification, Biogeosciences, 6, 2611–2623, doi:10.5194/bg-6-2611-2009, 2009. 3768

Rose, J. M. and Caron, D. A.: Does low temperature constrain the growth rates of heterotrophic protists? Evidence and implications for algal blooms in cold waters, Limnol. Oceanogr., 52, 886–895, doi:10.4319/lo.2007.52.2.0886, 2007. 3770

Ruggio, R., Vichi, M., Paparella, F., and Masina, S.: Climatic trends of the equatorial undercurrent: a backup mechanism for sustaining the equatorial Pacific production, J. Marine Syst., 121–122, 11–23, doi:10.1016/j.jmarsys.2013.04.001, 2013. 3749, 3764

Rykaczewski, R. R. and Dunne, J. P.: A measured look at ocean chlorophyll trends, Nature, 472, E5–E6, doi:10.1038/nature09952, 2011. 3735

Sailley, S., Vogt, M., Doney, S., Aita, M., Bopp, L., Buitenhuis, E., Hashioka, T., Lima, I., Le Quéré, C., and Yamanaka, Y.: Comparing food web structures and dynamics across a suite of global marine ecosystem models, Ecol. Model., 261–262, 43–57, doi:10.1016/j.ecolmodel.2013.04.006, 2013. 3738

Sand-Jensen, K., Pedersen, N. L., and Søndergaard, M.: Bacterial metabolism in small temperate streams under contemporary and future climates, Freshwater Biol., 52, 2340–2353, doi:10.1111/j.1365-2427.2007.01852.x, 2007. 3770

Sarmiento, J. L. and Gruber, N.: Ocean Biogeochemical Dynamis, Princeton University Press, Princeton, 2006. 3734

Sarmiento, J. L., Slater, R., Barber, R., Bopp, L., Doney, S. C., Hirst, A., Kleypas, J., Matear, R., Mikolajewicz, U., Monfray, P., Soldatov, V., Spall, S., and Stouffer, R.: Response of ocean ecosystems to climate warming, Global Biogeochem. Cy., 18, GB3003, doi:10.1029/2003GB002134, 2004. 3734, 3760

Schmittner, A. and Galbraith, E. D.: Glacial greenhouse-gas fluctuations controlled by ocean circulation changes, Nature, 456, 373–376, doi:10.1038/nature07531, 2008. 3760

Schmittner, A., Oschlies, A., Matthews, H. D., and Galbraith, E. D.: Future changes in climate, ocean circulation, ecosystems, and biogeochemical cycling simulated for a business-as-usual CO_2 emission scenario until year 4000 AD, Global Biogeochem. Cy., 22, GB1013, doi:10.1029/2007GB002953, 2008. 3734, 3735

Séférian, R., Bopp, L., Gehlen, M., Orr, J. C., Ethé, C., Cadule, P., Aumont, O., Salas y Mélia, D., Voldoire, A., and Madec, G.: Skill assessment of three earth system models with common marine biogeochemistry, Clim. Dynam., 40, 2549–2573, doi:10.1007/s00382-012-1362-8, 2013. 3762, 3796

Shigemitsu, M., Okunishi, T., Nishioka, J., Sumata, H., Hashioka, T., Aita, M. N., Smith, S. L., Yoshie, N., Okada, N., and Yamanaka, Y.: Development of a one-dimensional ecosystem model including the iron cycle applied to the Oyashio region, western subarctic Pacific, J. Geophys. Res., 117, C06021, doi:10.1029/2011JC007689, 2012. 3796

Siegel, D., Behrenfeld, M., Maritorena, S., McClain, C., Antoine, D., Bailey, S., Bontempi, P., Boss, E., Dierssen, H., Doney, S., Eplee, R., Evans, R., Feldman, G., Fields, E., Franz, B., Kuring, N., Mengelt, C., Nelson, N., Patt, F., Robinson, W., Sarmiento, J., Swan, C., Werdell, P., Westberry, T., Wilding, J., and Yoder, J.: Regional to global assessments of phytoplankton dynamics from the SeaWiFS mission, Remote Sens. Environ., 135, 77–91, doi:10.1016/j.rse.2013.03.025, 2013. 3766

Sinha, B., Buitenhuis, E. T., Quéré, C. L., and Anderson, T. R.: Comparison of the emergent behavior of a complex ecosystem model in two ocean general circulation models, Prog. Oceanogr., 84, 204–224, doi:10.1016/j.pocean.2009.10.003, 2010. 3763

Smith, S., Yamanaka, Y., Pahlow, M., and Oschlies, A.: Optimal uptake kinetics: physiological acclimation explains the pattern of nitrate uptake by phytoplankton in the ocean, Mar. Ecol.-Prog. Ser., 384, 1–12, doi:10.3354/meps08022, 2009. 3740

Steinacher, M., Joos, F., Frölicher, T. L., Bopp, L., Cadule, P., Cocco, V., Doney, S. C., Gehlen, M., Lindsay, K., Moore, J. K., Schneider, B., and Segschneider, J.: Projected 21st century decrease in marine productivity: a multi-model analysis, Biogeosciences, 7, 979–1005, doi:10.5194/bg-7-979-2010, 2010. 3734, 3735, 3736, 3746, 3758, 3759, 3760

Tagliabue, A., Bopp, L., and Gehlen, M.: The response of marine carbon and nutrient cycles to ocean acidification: large uncertainties related to phytoplankton physiological assumptions, Global Biogeochem. Cy., 25, GB3017, doi:10.1029/2010GB003929, 2011. 3768

Taucher, J. and Oschlies, A.: Can we predict the direction of marine primary production change under global warming?, Geophys. Res. Lett., 38, 1–6, doi:10.1029/2010GL045934, 2011. 3734, 3760, 3766

Taylor, K. E., Stouffer, R. J., and Meehl, G. A.: An overview of CMIP5 and the experiment design, B. Am. Meteorol. Soc., 93, 485–498, doi:10.1175/BAMS-D-11-00094.1, 2012. 3738

The HadGEM2 Development Team: G. M. Martin, Bellouin, N., Collins, W. J., Culverwell, I. D., Halloran, P. R., Hardiman, S. C., Hinton, T. J., Jones, C. D., McDonald, R. E., McLaren, A. J., O'Connor, F. M., Roberts, M. J., Rodriguez, J. M., Woodward, S., Best, M. J., Brooks, M. E., Brown, A. R., Butchart, N., Dearden, C., Derbyshire, S. H., Dharssi, I., Doutriaux-Boucher, M., Edwards, J. M., Falloon, P. D., Gedney, N., Gray, L. J., Hewitt, H. T., Hobson, M., Huddleston, M. R., Hughes, J., Ineson, S., Ingram, W. J., James, P. M., Johns, T. C., Johnson, C. E., Jones, A., Jones, C. P., Joshi, M. M., Keen, A. B., Liddicoat, S., Lock, A. P., Maidens, A. V., Manners, J. C., Milton, S. F., Rae, J. G. L., Ridley, J. K., Sellar, A., Senior, C. A., Totterdell, I. J., Verhoef, A., Vidale, P. L., and Wiltshire, A.: The HadGEM2 family of Met Office Unified Model climate configurations, Geosci. Model Dev., 4, 723–757, doi:10.5194/gmd-4-723-2011, 2011. 3796

Toseland, A., Daines, S. J., Clark, J. R., Kirkham, A., Strauss, J., Uhlig, C., Lenton, T. M., Valentin, K., Pearson, G. A., Moulton, V., and Mock, T.: The impact of temperature on marine phytoplankton resource allocation and metabolism, Nature Climate Change, 3, 979–984, doi:10.1038/nclimate1989, 2013. 3768, 3771

Totterdell, I.: Description of Diat-HadOCC, Tech. rep., MetOffice, Exeter, UK, 2013. 3796

van Vuuren, D. P., Edmonds, J., Kainuma, M., Riahi, K., Thomson, A., Hibbard, K., Hurtt, G. C., Kram, T., Krey, V., Lamarque, J.-F., Masui, T., Meinshausen, M., Nakicenovic, N., Smith, S. J., and Rose, S. K.: The representative concentration pathways: an overview, Climatic Change, 109, 5–31, doi:10.1007/s10584-011-0148-z, 2011. 3737

Vancoppenolle, M., Bopp, L., Madec, G., Dunne, J., Ilyina, T., Halloran, P. R., and Steiner, N.: Future Arctic Ocean primary productivity from CMIP5 simulations: uncertain outcome, but consistent mechanisms, Global Biogeochem. Cy., 27, 605–619, doi:10.1002/gbc.20055, 2013. 3757

Vichi, M., Pinardi, N., and Masina, S.: A generalized model of pelagic biogeochemistry for the global ocean ecosystem. Part I: Theory, J. Marine Syst., 64, 89–109, doi:10.1016/j.jmarsys.2006.03.006, 2007. 3742, 3780, 3796

Vichi, M., Allen, J. I., Masina, S., and Hardman-Mountford, N. J.: The emergence of ocean biogeochemical provinces: a quantitative assessment and a diagnostic for model evaluation, Global Biogeochem. Cy., 25, 1–17, doi:10.1029/2010GB003867, 2011a. 3749, 3796

Vichi, M., Manzini, E., Fogli, P. G., Alessandri, A., Patara, L., Scoccimarro, E., Masina, S., and Navarra, A.: Global and regional ocean carbon uptake and climate change: sensitivity to a substantial mitigation scenario, Clim. Dynam., 37, 1929–1947, doi:10.1007/s00382-011-1079-0, 2011b. 3764

Vogt, M., Hashioka, T., Payne, M. R., Buitenhuis, E. T., Quéré, C. Le, Alvain, S., Aita, M. N., Bopp, L., Doney, S. C., Hirata, T., Lima, I., Sailley, S., and Yamanaka, Y.: The distribution, dominance patterns and ecological niches of plankton functional types in Dynamic Green Ocean Models and satellite estimates, Biogeosciences Discuss., 10, 17193–17247, doi:10.5194/bgd-10-17193-2013, 2013. 3738

Voldoire, A., Sanchez-Gomez, E., Salas y Mélia, D., Decharme, B., Cassou, C., Sénési, S., Valcke, S., Beau, I., Alias, A., Chevallier, M., Déqué, M., Deshayes, J., Douville, H., Fernandez, E., Madec, G., Maisonnave, E., Moine, M.-P., Planton, S., Saint-Martin, D., Szopa, S., Tyteca, S., Alkama, R., Belamari, S., Braun, A., Coquart, L., and Chauvin, F.: The CNRM-CM5.1 global climate model: description and basic evaluation, Clim. Dynam., 40, 2091–2121, doi:10.1007/s00382-011-1259-y, 2012. 3796

Watanabe, S., Hajima, T., Sudo, K., Nagashima, T., Takemura, T., Okajima, H., Nozawa, T., Kawase, H., Abe, M., Yokohata, T., Ise, T., Sato, H., Kato, E., Takata, K., Emori, S., and Kawamiya, M.: MIROC-ESM 2010: model description and basic results of CMIP5-20c3m experiments, Geosci. Model Dev., 4, 845–872, doi:10.5194/gmd-4-845-2011, 2011. 3796

Webb, W. L., Newton, M., and Starr, D.: Carbon dioxide exchange of Alnus rubra, Oecologia, 17, 281–291, doi:10.1007/BF00345747, 1974. 3741

Wernand, M. R., van der Woerd, H. J., and Gieskes, W. W. C.: Trends in ocean colour and chlorophyll concentration from 1889 to 2000, worldwide, PLOS one, 8, e63766, doi:10.1371/journal.pone.0063766, 2013. 3735

Westberry, T., Behrenfeld, M. J., Siegel, D. A., and Boss, E.: Carbon-based primary productivity modeling with vertically resolved photoacclimation, Global Biogeochem. Cy., 22, GB2024, doi:10.1029/2007GB003078, 2008. 3744, 3802, 3812, 3824

Williams, P. J. L. B., Quay, P. D., Westberry, T. K., and Behrenfeld, M. J.: The oligotrophic ocean is autotrophic, Annual Review of Marine Science, 5, 535–49, doi:10.1146/annurev-marine-121211-172335, 2013. 3770

Table 1. Overview of model simulations used in this work.

Earth System Model	Reference	Ocean model	Ecosystem model	Reference	Spin-up (years, offline + online)	Project	Coupling
HadGEM2-ES	Collins et al. (2011), HadGEM Team et al. (2011)	MetUM	diat-HadOCC	Totterdell (2013)	CMIP3 + 500 + 100	CMIP5	fully coupled
CESM1	Hurrell et al. (2013), Lindsay et al. (2014)	POP	BEC	Moore et al. (2013b)	1025 + 150	MAREMIP	fully coupled
GFDL-ESM2M	Dunne et al. (2012, 2013)	MOM	TOPAZ	Dunne et al. (2013)	1 + 1000	MAREMIP	fully coupled
IPSL-CM5A-LR	Dufresne et al. (2013)	NEMO	PISCES	Aumont and Bopp (2006)	3000 + 300	CMIP5	fully coupled
CNRM-CM5	Voldoire et al. (2012)	NEMO	PISCES	Aumont and Bopp (2006) [a]	3000 + 300	CMIP5	fully coupled
MIROC5	Watanabe et al. (2011)	MRI.COM	MEM	Shigemitsu et al. (2012)	1245 + 480	MAREMIP	ocean only
CMCC-CESM	Vichi et al. (2011a) Cagnazzo et al. (2013)	NEMO	PELAGOS	Vichi et al. (2007)	1 + 450[b]	CMIP5	fully coupled
MIROC5	Watanabe et al. (2011)	MITgcm	REcoM2	Hauck et al. (2013)	0 +112	MAREMIP	ocean only
IPSL-CM5A-LR	Dufresne et al. (2013)	NEMO	PlankTOM5.3	Buitenhuis et al. (2013a)	0 + 6	MAREMIP	ocean only

[a] For differences between the two PISCES simulations see Séférian et al. (2013).

[b] Land and ocean carbon pools have been adjusted to the atmospheric preindustrial CO_2 with an acceleration method described in Vichi et al. (2011a).

Table 2. Overview of ecosystem models used in this work, extended from Bopp et al. (2013).

Ecosystem model	Nutrients	Phytoplankton types	Zooplankton types	Stochiometry
diat-HadOCC	4 (NO_3, NH_4, SiO_4,Fe)	2 (diatom, non-diatom); implicit calcification	1	R(C : N), V(Si, Fe)
REcoM2	4 (NO_3, SiO_4,Fe)	2 (diatom, nano-, implicit calcification)	1	V(C,N,Si,Chl), (C : Fe) fix
BEC	5 (NO_3, NH_4, PO_4,SiO_4,Fe)	3 (diatom, nano-, diazotroph, implicit calcification)	1	R(C : N : P), V(Si,Chl,Fe)
TOPAZ	5 (NO_3, NH_4, PO_4,SiO_4,Fe)	3 (large separated into diatoms and other eukaryotes, nano-, diazotrophs, implicit calcification)	(implicit)	R(C : N), V(P, Si, Chl, Fe)
PISCES	5 (NO_3, NH_4, PO_4,SiO_4,Fe)	2 (diatom, nano-, implicit calcification)	2 (micro- and mesozooplankton)	R(C : N : P), V(Si, Chl, Fe)
MEM	4 (NO_3, NH_4 SiO_4,Fe)	2 (diatom, nanophytoplankton)	3 (micro-, meso-, predatory zooplankton)	R(C : N : P), Chl, Si, Fe fix
PELAGOS	5 (NO_3, NH_4, PO_4,SiO_4,Fe)	3 (diatoms, flagellates, picophytoplankton)	3 (micro-,mesozooplankton, heterotrophic nanoflagellates)	V(N,P,Si,Chl,Fe)
PlankTOM5.3	3 (NO_3, SiO_4,Fe)	3 (diatoms, nanophytoplankton, coccolithophores)	2 (micro-, mesozooplankton)	R(C : N), V(Si, Chl, Fe)

Table 3. Comparison of temperature limitations in ecosystem models.

Ecosystem model	Q_{10}
Diat-HadOCC	None
REcoM2	15 to 25 °C: 1.69, 0 to 10 °C: 1.79
BEC	2.0
TOPAZ	1.87
PISCES	1.89, mesozooplankton: 2.14
MEM	2.0
PELAGOS	2.0, mesozooplankton: 3.0
PlankTOM5.3	cocco: 1.68, diatoms: 1.93, nano: 2.08 micro: 1.77, meso: 1.71

Table 4. Comparison of nutrient limitation of phytoplankton growth in ecosystem models.

Ecosystem model	Nutrient limitation
Diat-HadOCC	Michaelis–Menten, multiplicative iron limitation
REcoM2	Cell quota, Fe with Michaelis–Menten
BEC	Michaelis–Menten
TOPAZ	Cell quota
PISCES	Michaelis–Menten
MEM	Optimal uptake kinetics
PELAGOS	Multiplicative, cell quota, included in exudation term
PlankTOM5.3	Fe with cell quota, Si, NO_3 Michaelis–Menten and μ_{max} depends on Fe and Chl cell quota

Table 5. Comparison of prey dependence of grazing. $K_{1/2}$ is a Michaelis–Menten constant, p is the food preference and vp stands for variable food preference. For the full equations see Appendix. A

Ecosystem model	Prey dependence	Prey
Diat-HadOCC	$\frac{\mathrm{vp}\cdot P}{K_{1/2}+\mathrm{Food}}$	$\mathrm{Food} = \mathrm{vp}_{\mathrm{diat}} \cdot \mathrm{diatoms} + \mathrm{vp}_{\mathrm{nano}} \cdot \mathrm{nanos} + \mathrm{vp}_{\mathrm{detr}} \cdot \mathrm{detritus}$
REcoM2	$\frac{\mathrm{Food}^2}{K_{1/2}+\mathrm{Food}^2}$	$\mathrm{Food} = \mathrm{nano} + p_{\mathrm{diat}} \cdot \mathrm{diatoms}$
BEC	$\frac{P^2}{K_{1/2}+P^2}$	P = diatoms, nanos, diazotrophs
TOPAZ	implicit zoo, see Appendix A	diatoms, nanos, diazotrophs, large phyto
PISCES	see Appendix A	Food = diatoms, nanos, detritus, microzooplankton
MEM	$1 - e^{(\mathrm{Ivlev}\cdot(P^* - P))}$	P = diatoms, nanos, micro-, mesozooplankton
PELAGOS	$\frac{\mathrm{vp}\cdot P}{K_{1/2}+\mathrm{Food}}$	diatoms, nanos, picos, flagellates, micro-, mesozoopl.
PlankTOM5.3	$\frac{p\cdot P}{K_{1/2}+\mathrm{Food}}$	$\mathrm{Food} = p_{\mathrm{dia}} \cdot \mathrm{dia} + p_{\mathrm{nan}} \cdot \mathrm{nan} + p_{\mathrm{coc}} \cdot \mathrm{coc} + p_{\mathrm{detr}} \cdot \mathrm{detr} + p_{\mathrm{mic}} \cdot \mathrm{micro}$

Title Page
Abstract Introduction
Conclusions References
Tables Figures
◀◀ ▶▶
◀ ▶
Back Close
Full Screen / Esc
Printer-friendly Version
Interactive Discussion

Table 6. NPP changes (total and in %) in different regions. The Pacific upwelling region is shown in Fig. 3. Changes describe the difference between the 2012–2031 and the 2081–2100 average.

Region	Area in %	NPP in %	multimodel median	Change (Gt C yr^{-1})	multimodel median change (Gt C yr^{-1})
global	100	100	100	−4.3 to +10	−0.2
low latitudes	53	40–65	58	−3.9 to +9.9	−0.3
Pacific upwelling	15	14–33	20	−2.2 to +2.3	−0.36
S. Ocean (< 50° S)	12	6.5–19	9	−0.01 to +0.4	+0.24
S. Intermediate (30–50° S)	18	13–27	18	−0.7 to +0.27	−0.01
N. Hemisphere (30–90° N)	16	11–17	14	−0.6 to +0.39	−0.1

Table 7. Model skill in representing global NPP, measured in Spearman's rank correlation, normalized SD (NStdDev) and bias. The NPP data is from Westberry et al. (2008), the average global NPP value is 12.6 mol C m^{-2} yr^{-1}. The chlorophyll data is from the SeaWiFS Project, the average global chlorophyll value is 0.28 mg Chl m^{-3}.

Model simulation	Correlation	NStdDev	Bias
Integrated NPP [mol C m^{-2} yr^{-1}]			
Diat-HadOCC	0.18	1.20	−4.5
REcoM2	0.33	0.84	−6.54
BEC	0.67	0.95	−0.56
TOPAZ	0.69	1.49	6.80
CNRM/PISCES	0.09	0.78	−7.94
IPSL/PISCES	0.39	0.80	−4.65
MEM	0.49	1.14	−8.87
PELAGOS	0.40	1.04	−4.47
PlankTOM5.3	0.54	0.92	−0.47
Surface chlorophyll [mg Chl m^{-3}]			
Diat-HadOCC	0.52	0.62	0.61
REcoM2	0.62	0.19	−0.02
BEC	0.66	0.40	0.01
TOPAZ	0.72	0.14	0.04
CNRM/PISCES	0.58	0.23	−0.13
IPSL/PISCES	0.54	0.19	−0.09
MEM	0.58	0.14	−0.03
PELAGOS	0.36	0.44	−0.02
PlankTOM5.3	0.50	1.35	2.69

Table 8. Model skill in representing surface nutrients, measured in Pearson correlation, normalized SD (NStdDev) and bias. Nutrient data from Garcia et al. (2014). The average global values for NO_3, SiO_3 and PO_4 are 6.7 mmol NO_3 m^{-3}, 10.6 mmol SiO_3 m^{-3}, and 0.66 mmol PO_4 m^{-3}, respectively.

Model simulation	Correlation	NStdDev	Bias
Surface NO_3 [mmol N m^{-3}]			
Diat-HadOCC	0.83	1.01	−0.51
REcoM2	0.67	0.86	3.60
BEC	0.84	0.91	0.23
TOPAZ	0.83	0.99	1.43
CNRM/PISCES	0.62	1.10	4.89
IPSL/PISCES	0.83	0.91	−0.69
MEM	0.84	1.10	0.82
PELAGOS	0.72	0.19	−4.24
PlankTOM5.3	0.85	1.01	3.23
Surface SiO_3 [mmol Si m^{-3}]			
Diat-HadOCC	0.45	0.83	45.11
REcoM2	0.56	0.62	−5.24
BEC	0.61	0.75	−0.17
TOPAZ	0.62	1.36	4.63
CNRM/PISCES	0.66	0.60	−0.97
IPSL/PISCES	0.50	1.01	2.75
MEM	0.76	1.47	6.58
PELAGOS			
PlankTOM5.3	0.51	0.85	−6.87
Surface PO_4 [mmol P m^{-3}]			
BEC	0.87	0.93	0.03
TOPAZ	0.83	0.99	−0.10
CNRM/PISCES	0.82	0.99	−0.32
IPSL/PISCES	0.85	1.05	−0.17
PELAGOS	0.77	13.51	5.20

Table A1. Symbols used in the model equations.

Symbol	Meaning
T_f	Temperature limitation factor
N_lim	Nutrient limitation factor
L_lim	Light limitation factor
μ_i	Growth rate of phytoplankton *i*
T	Temperature in °C
$\theta_\mathrm{Chl/C}$	Chlorophyll to Carbon ratio
I_PAR	Photosynthetically active radiation
Fe	Iron concentration
PO_4	Phosphate concentration
NH_4	Ammonium concentration
NO_3	Nitrate concentration
SiO_3	Silicate concentration

Table A2. BEC parameters.

Parameter	Value	Unit	Description
Q_{10}	2		temperature dependence factor
T_{ref}	30	°C	reference temperature
α^{diat}	0.3	$\mathrm{mmol\,C\,m^2\,(mg\,Chl\,W\,day)^{-1}}$	initial slope of P-I curve
α^{nano}	0.3	$\mathrm{mmol\,C\,m^2\,(mg\,Chl\,W\,day)^{-1}}$	initial slope of P-I curve
$\mu_{\mathrm{max}}^{\mathrm{diat}}$	3.0	$\mathrm{day^{-1}}$	max. phytoplankton growth rate at T_{ref}
$\mu_{\mathrm{max}}^{\mathrm{nano}}$	3.0	$\mathrm{day^{-1}}$	max. phytoplankton growth rate at T_{ref}
$K_{\mathrm{NH_4}}^{\mathrm{diat}}$	0.08	$\mathrm{mmol\,N\,m^{-3}}$	NH_4 half saturation coefficient
$K_{\mathrm{NH_4}}^{\mathrm{nano}}$	0.005	$\mathrm{mmol\,N\,m^{-3}}$	NH_4 half saturation coefficient
$K_{\mathrm{NO_3}}^{\mathrm{diat}}$	2.5	$\mathrm{mmol\,N\,m^{-3}}$	NO_3 half saturation coefficient
$K_{\mathrm{NO_3}}^{\mathrm{nano}}$	0.5	$\mathrm{mmol\,N\,m^{-3}}$	NO_3 half saturation coefficient
$K_{\mathrm{PO_4}}^{\mathrm{diat}}$	0.005	$\mathrm{mmol\,PO_4\,m^{-3}}$	PO_4 half saturation coefficient
$K_{\mathrm{PO_4}}^{\mathrm{nano}}$	3.125×10^{-4}	$\mathrm{mmol\,PO_4\,m^{-3}}$	PO_4 half saturation coefficient
$K_{\mathrm{Fe}}^{\mathrm{diat}}$	1.5×10^{-4}	$\mathrm{mmol\,Fe\,m^{-3}}$	Fe half saturation coefficient
$K_{\mathrm{Fe}}^{\mathrm{nano}}$	6×10^{-5}	$\mathrm{mmol\,Fe\,m^{-3}}$	Fe half saturation coefficient
$K_{\mathrm{SiO_3}}^{\mathrm{diat}}$	1.0	$\mathrm{mmol\,SiO_3\,m^{-3}}$	SiO_3 half saturation coefficient

Table A3. TOPAZ parameters.

Parameter	Value	Unit	Description
ζ	0.1		photorespiration loss
K_{Eppley}	0.063	$^{\circ}\mathrm{C}^{-1}$	temperature dependence factor
α^{diat}	$\frac{2.4\times10^{-5}\cdot2.77\times10^{18}}{6.022\times10^{17}}$	$\mathrm{g\,C\,m^2\,(g\,Chl\,W\,s)^{-1}}$	initial slope of P-I curve
α^{nano}	$\frac{2.4\times10^{-5}\cdot2.77\times10^{18}}{6.022\times10^{17}}$	$\mathrm{g\,C\,m^2\,(g\,Chl\,W\,s)^{-1}}$	initial slope of P-I curve
$\mu_{\mathrm{max}}^{\mathrm{diat}}$	1.5×10^{-5}	$\mathrm{s^{-1}}$	max. phytoplankton growth rate at 0 °C
$\mu_{\mathrm{max}}^{\mathrm{nano}}$	1.5×10^{-5}	$\mathrm{s^{-1}}$	max. phytoplankton growth rate at 0 °C
$Q_{\mathrm{min}}^{\mathrm{nolim}}$	0.01	$\mathrm{g\,Chl\,(g\,C)^{-1}}$	min. Chl : C without nutrient limitation
$Q_{\mathrm{min}}^{\mathrm{lim}}$	0.001	$\mathrm{g\,Chl\,(g\,C)^{-1}}$	min. Chl : C with complete nutrient limitation
$Q_{\mathrm{max}}^{\mathrm{nano}}$	0.04	$\mathrm{g\,Chl\,(g\,C)^{-1}}$	max. Chl : C
$Q_{\mathrm{max}}^{\mathrm{large}}$	0.06	$\mathrm{g\,Chl\,(g\,C)^{-1}}$	max. Chl : C
$K_{\mathrm{NH_4}}^{\mathrm{large}}$	2×10^{-7}	$\mathrm{mol\,N\,kg^{-1}}$	$\mathrm{NH_4}$ half saturation coefficient
$K_{\mathrm{NH_4}}^{\mathrm{nano}}$	6×10^{-7}	$\mathrm{mol\,N\,kg^{-1}}$	$\mathrm{NH_4}$ half saturation coefficient
$K_{\mathrm{NO_3}}^{\mathrm{large}}$	6×10^{-6}	$\mathrm{mol\,N\,kg^{-1}}$	$\mathrm{NO_3}$ half saturation coefficient
$K_{\mathrm{NO_3}}^{\mathrm{nano}}$	2×10^{-6}	$\mathrm{mol\,N\,kg^{-1}}$	$\mathrm{NO_3}$ half saturation coefficient
$K_{\mathrm{SiO_3}}^{\mathrm{diat}}$			$\mathrm{SiO_3}$ half saturation coefficient
$Q_{\mathrm{Fe:N,\,max}}^{\mathrm{large}}$	$666\times10^{-6}\cdot\frac{106}{16}$	$\mathrm{mol\,Fe\,(mol\,N)^{-1}}$	maximum Fe : N limit
$Q_{\mathrm{Fe:N,\,max}}^{\mathrm{nano}}$	$46\times10^{-6}\cdot\frac{106}{16}$	$\mathrm{mol\,Fe\,(mol\,N)^{-1}}$	maximum Fe : N limit
$Q_{\mathrm{P:N,\,max}}^{\mathrm{large}}$	0.1236	$\mathrm{mol\,P\,(mol\,N)^{-1}}$	maximum P : N limit
$Q_{\mathrm{P:N,\,max}}^{\mathrm{nano}}$	0.1458	$\mathrm{mol\,P\,(mol\,N)^{-1}}$	maximum P : N limit
$k_{\mathrm{graz_{max}}}$			
u_{max}	0.19/86 400	$\mathrm{s^{-1}}$	grazing rate at 0 °C
$P^{\star}$	$1.9\times10^{-6}\cdot\frac{16}{106}$	$\mathrm{mol\,N\,kg^{-1}}$	pivot phyto concentration for grazing allometry
P_{min}	1×10^{-10}	$\mathrm{mol\,N\,kg^{-1}}$	min. phyto concentration threshold for grazing

Table A4. PISCES parameters.

Parameter	Value	Unit	Description
k_{Eppley}	0.063913	$^\circ\mathrm{C}^{-1}$	temperature dependence factor
$k_{\text{Eppley, meso}}$	0.07608	$^\circ\mathrm{C}^{-1}$	temp. dependence factor mesozooplankton
α	3.0	$(\mathrm{W\,m^2})^{-1}\,\mathrm{day}^{-1}$	initial slope of P-I curve
β^{nano}	1.0	m	Coefficient for mixed layer depth influence
β^{diat}	3.0	m	Coefficient for mixed layer depth influence
μ_{max}	0.6	day^{-1}	max. phytoplankton growth rate
$K^{\text{diat}}_{\mathrm{NH_4}}$	5×10^{-7}	$\mathrm{mol\,N\,L^{-1}}$	NH_4 half saturation coefficient
$K^{\text{nano}}_{\mathrm{NH_4}}$	1×10^{-7}	$\mathrm{mol\,N\,L^{-1}}$	NH_4 half saturation coefficient
$K^{\text{diat}}_{\mathrm{NO_3}}$	10×10^{-6}	$\mathrm{mol\,N\,L^{-1}}$	NO_3 half saturation coefficient
$K^{\text{nano}}_{\mathrm{NO_3}}$	2×10^{-6}	$\mathrm{mol\,N\,L^{-1}}$	NO_3 half saturation coefficient
$K^{\text{diat}}_{\mathrm{PO_4}}$	1×10^{-7}	$\mathrm{mol\,PO_4\,L^{-1}}$	PO_4 half saturation coefficient
$K^{\text{nano}}_{\mathrm{PO_4}}$	1×10^{-7}	$\mathrm{mol\,PO_4\,L^{-1}}$	PO_4 half saturation coefficient
$K^{\text{diat}}_{\text{Fe, min}}$	1×10^{-10}	$\mathrm{mol\,Fe\,L^{-1}}$	min. Fe half saturation coefficient
$K^{\text{nano}}_{\text{Fe, min}}$	2×10^{-11}	$\mathrm{mol\,Fe\,L^{-1}}$	min. Fe half saturation coefficient
$K^{\text{diat}}_{\text{Fe}}$	4×10^{-10}	$\mathrm{mol\,Fe\,L^{-1}}$	Fe half saturation coefficient
$K^{\text{nano}}_{\text{Fe}}$	8×10^{-11}	$\mathrm{mol\,Fe\,L^{-1}}$	Fe half saturation coefficient
$K^{\text{diat}}_{\mathrm{SiO_3}}$	3.33×10^{-6}	$\mathrm{mol\,SiO_3\,L^{-1}}$	SiO_3 half saturation coefficient
$u^{\text{meso}\rightarrow\text{nano}}_{\text{max}}$	0.7	day^{-1}	max. meso zoo. growth rate on nanos
$u^{\text{micro}\rightarrow\text{nano}}_{\text{max}}$	4.0	day^{-1}	max. micro zoo. growth rate on nanos
K_{G}	20×10^{-6}	$\mathrm{mol\,C\,L^{-1}}$	half-saturation constant for grazing
$\Psi^{\text{micro}}_{\text{nano}}$	0.5		preference coefficient for micro grazing on nanos
$\Psi^{\text{micro}}_{\text{diat}}$	0.5		preference coefficient for micro grazing on diatoms
$\Psi^{\text{meso}}_{\text{nano}}$	0.2		preference coefficient for meso grazing on nanos
$\Psi^{\text{meso}}_{\text{diat}}$	1.0		preference coefficient for meso grazing on diatoms
$\Psi^{\text{meso}}_{\text{micro}}$	1.0		preference coefficient for meso grazing on micro

Table A5. MEM parameters.

Parameter	Value	Unit	Description
k_{Eppley}	0.0639	°C^{-1}	temperature dependence factor
$\mu_{\mathrm{max}}^{\mathrm{diat}}$	1.2	day^{-1}	max. phytoplankton growth rate at T_{ref}
$\mu_{\mathrm{max}}^{\mathrm{nano}}$	0.6	day^{-1}	max. phytoplankton growth rate at T_{ref}
α^{diat}	0.045	(W m^{-2})$^{-1}$ day^{-1}	Initial slope of P-I curve
α^{nano}	0.013	(W m^{-2})$^{-1}$ day^{-1}	Initial slope of P-I curve
β	1.4×10^{-15}	(W m^{-2})$^{-1}$ day^{-1}	Photoinhibition index
P_S^{diat}	1.4	day^{-1}	Potential maximum light saturated photosynthetic rate
P_S^{nano}	0.4	day^{-1}	Potential maximum light saturated photosynthetic rate
$K_{\mathrm{NH_4}}^{\mathrm{diat}}$	0.3	µmol L^{-1}	NH_4 Half-saturation coefficient
$K_{\mathrm{NH_4}}^{\mathrm{nano}}$	0.1×10^{-6}	µmol L^{-1}	NH_4 half-saturation coefficient
$A_{\mathrm{NO_3}}^{\mathrm{diat}}$	10.0	(mol N)$^{-1}$ s^{-1}	Potential maximum affinity for NO_3
$A_{\mathrm{NO_3}}^{\mathrm{nano}}$	30.0	(mol N)$^{-1}$ s^{-1}	Potential maximum affinity for NO_3
$A_{\mathrm{NH_4}}^{\mathrm{diat}}$	100.0	(mol N)$^{-1}$ s^{-1}	Potential maximum affinity for NH_4
$A_{\mathrm{NH_4}}^{\mathrm{nano}}$	300.0	(mol N)$^{-1}$ s^{-1}	Potential maximum affinity for NH_4
$A_{\mathrm{Fe}}^{\mathrm{diat}}$	1.111×10^{-5}	(mol Fe)$^{-1}$ s^{-1}	Potential maximum affinity for Fe
$A_{\mathrm{Fe}}^{\mathrm{nano}}$	2.5×10^{-5}	(mol Fe)$^{-1}$ s^{-1}	Potential maximum affinity for Fe
$A_{\mathrm{SiO_3}}^{\mathrm{diat}}$	1.6666	(mol SiO_3)$^{-1}$ s^{-1}	Potential maximum affinity for SiO_3
$u_{\mathrm{max}}^{\mathrm{micro \to nano}}$	0.4	day^{-1}	Max. micro zoo. growth rate on nanos at 0 °C
$u_{\mathrm{max}}^{\mathrm{meso \to nano}}$	0.1	day^{-1}	Max. meso zoo. growth rate on nanos at 0 °C
$u_{\mathrm{max}}^{\mathrm{meso \to diat}}$	0.4	day^{-1}	Max. meso zoo. growth rate on diatoms at 0 °C
$u_{\mathrm{max}}^{\mathrm{meso \to micro}}$	0.4	day^{-1}	Max. meso zoo. growth rate on micro zoo. at 0 °C
$u_{\mathrm{max}}^{\mathrm{pred \to diat}}$	0.2	day^{-1}	Max. pred zoo. growth rate on diatoms at 0 °C
$u_{\mathrm{max}}^{\mathrm{pred \to micro}}$	0.2	day^{-1}	Max. pred zoo. growth rate on micro zoo. at 0 °C
$u_{\mathrm{max}}^{\mathrm{pred \to meso}}$	0.4	day^{-1}	Max. pred zoo. growth rate on meso zoo. at 0 °C
$T_{\mathrm{nano}}^{\mathrm{micro}}$	0.043	µmol N L^{-1}	Threshold value for micro. zoo. grazing on nanos
$T_{\mathrm{nano}}^{\mathrm{meso}}$	0.04	µmol N L^{-1}	Threshold value for meso. zoo. grazing on nanos
$T_{\mathrm{diat}}^{\mathrm{meso}}$	0.04	µmol N L^{-1}	Threshold value for meso. zoo. grazing on diatoms
$T_{\mathrm{micro}}^{\mathrm{meso}}$	0.04	µmol N L^{-1}	Threshold value for meso. zoo. grazing on micro zoo.
$T_{\mathrm{diat}}^{\mathrm{pred}}$	0.04	µmol N L^{-1}	Threshold value for pred. zoo. grazing on diatoms
$T_{\mathrm{micro}}^{\mathrm{pred}}$	0.04	µmol N L^{-1}	Threshold value for pred. zoo. grazing on micro zoo
$T_{\mathrm{meso}}^{\mathrm{pred}}$	0.04	µmol N L^{-1}	Threshold value for pred. zoo. grazing on meso zoo
λ	1.4	L (µmol N)$^{-1}$	Ivlev constant (all zoo PFTs)
Ψ_{micro}	3.01	L (µmol N)$^{-1}$	Preference coefficient for predation on micro zoo
Ψ_{meso}	4.605	L (µmol N)$^{-1}$	Preference coefficient for predation on meso zoo

Table A6. PELAGOS parameters.

Parameter	Value	Unit	Description
$\mu_{\text{max}}^{\text{diat}}$	3.0	day^{-1}	Max. phytoplankton growth rate
$\mu_{\text{max}}^{\text{nano}}$	3.0	day^{-1}	Max. phytoplankton growth rate
$\mu_{\text{max}}^{\text{pico}}$	3.0	day^{-1}	Max. phytoplankton growth rate
Q_{10}	2		temperature dependence factor
$Q_{10,\text{meso}}$	3		temperature dependence factor
α^{diat}	1.38×10^{-5}	$\text{mg C (mg Chl)}^{-1}\,\mu\text{E}^{-1}\,\text{m}^2\,\text{s}$	Maximal light utilization coefficient
α^{nano}	0.46×10^{-5}	$\text{mg C (mg Chl)}^{-1}\,\mu\text{E}^{-1}\,\text{m}^2\,\text{s}$	Maximal light utilization coefficient
α^{pico}	1.52×10^{-5}	$\text{mg C (mg Chl)}^{-1}\,\mu\text{E}^{-1}\,\text{m}^2\,\text{s}$	Maximal light utilization coefficient
u^{meso}	2.0	day^{-1}	Max. zoo. growth rate rate
u^{micro}	2.0	day^{-1}	Max. zoo. growth rate rate
$u^{\text{flagellates}}$	10.0	day^{-1}	Max. zoo. growth rate rate
$\delta_{\text{diat}}^{\text{micro}}$	0.2		Prey availability
$\delta_{\text{nano}}^{\text{micro}}$	1.0		Prey availability
$\delta_{\text{pico}}^{\text{micro}}$	0.1		Prey availability
$\delta_{\text{micro}}^{\text{micro}}$	1.0		Prey availability
$\delta_{\text{flagellates}}^{\text{micro}}$	0.8		Prey availability
$\delta_{\text{diat}}^{\text{meso}}$	1.0		Prey availability
$\delta_{\text{meso}}^{\text{meso}}$	1.0		Prey availability
$\delta_{\text{micro}}^{\text{meso}}$	1.0		Prey availability
$\delta_{\text{pico}}^{\text{flagellates}}$	0.9		Prey availability
$\delta_{\text{flagellates}}^{\text{flagellates}}$	0.2		Prey availability
e^{meso}	1		Capture efficiency
μ_{micro}	20.0	mg C m^{-3}	Feeding threshold
$\mu_{\text{flagellates}}$	20.0	mg C m^{-3}	Feeding threshold
$K_{1/2}^{\text{F,meso}}$	80	mg C m^{-3}	Grazing half-saturation constant
$K_{1/2}^{\text{F,micro}}$	20	mg C m^{-3}	Grazing half-saturation constant
$K_{1/2}^{\text{F,flagellates}}$	20	mg C m^{-3}	Grazing half-saturation constant

Table A7. PlankTOM5.3 parameters.

Parameter	Value	Unit	Description
$\mu_{\text{max}}^{\text{diat}}$	0.33	day^{-1}	Max. phytoplankton growth rate at 0 °C
$\mu_{\text{max}}^{\text{nano}}$	0.16	day^{-1}	Max. phytoplankton growth rate at 0 °C
$\mu_{\text{max}}^{\text{cocco}}$	0.23	day^{-1}	Max. phytoplankton growth rate at 0 °C
Q_{10}^{diat}	1.93		Temperature dependence factor
Q_{10}^{nano}	2.08		Temperature dependence factor
Q_{10}^{cocco}	1.68		Temperature dependence factor
Q_{10}^{micro}	1.71		Temperature dependence factor
Q_{10}^{meso}	3.18		Temperature dependence factor
α^{diat}	0.79×10^{-6}	$\text{mol C m}^2\,(\text{g Chl W d})^{-1}$	Initial slope of P-I curve
α^{nano}	0.83×10^{-6}	$\text{mol C m}^2\,(\text{g Chl W d})^{-1}$	Initial slope of P-I curve
α^{cocco}	1.25×10^{-6}	$\text{mol C m}^2\,(\text{g Chl W d})^{-1}$	Initial slope of P-I curve
$K_{\text{NO}_3}^{\text{diat}}$	50.0×10^{-6}	mol N m^{-3}	NO_3 Half saturation coefficient
$K_{\text{NO}_3}^{\text{nano}}$	9.2×10^{-6}	mol N m^{-3}	NO_3 Half saturation coefficient
$K_{\text{NO}_3}^{\text{nano}}$	3.0×10^{-6}	mol N m^{-3}	NO_3 Half saturation coefficient
$\theta_{\text{Fe/C,min}}^{\text{diat}}$	2.5×10^{-6}	$\text{mol Fe}\,(\text{mol C})^{-1}$	Minimum Fe : C ratio
$\theta_{\text{Fe/C,min}}^{\text{nano}}$	2.0×10^{-6}	$\text{mol Fe}\,(\text{mol C})^{-1}$	Minimum Fe : C ratio
$\theta_{\text{Fe/C,min}}^{\text{cocco}}$	3.7×10^{-6}	$\text{mol Fe}\,(\text{mol C})^{-1}$	Minimum Fe : C ratio
$\theta_{\text{Fe/C,opt}}^{\text{diat}}$	3.2×10^{-6}	$\text{mol Fe}\,(\text{mol C})^{-1}$	Optimal Fe : C ratio
$\theta_{\text{Fe/C,opt}}^{\text{nano}}$	3.0×10^{-6}	$\text{mol Fe}\,(\text{mol C})^{-1}$	Optimal Fe : C ratio
$\theta_{\text{Fe/C,opt}}^{\text{cocco}}$	5.9×10^{-6}	$\text{mol Fe}\,(\text{mol C})^{-1}$	Optimal Fe : C ratio
$K_{\text{SiO}_3}^{\text{diat}}$	4.0×10^{-6}	$\text{mol SiO}_3\text{ m}^{-3}$	SiO_3 Half saturation coefficient
$u_{\text{max}}^{\text{micro}}$		day^{-1}	Max. micro zoo. growth rate at 0 °C
$u_{\text{max}}^{\text{meso}}$		day^{-1}	Max. micro zoo. growth rate at 0 °C

Table A8. REcoM2 parameters.

Parameter	Value	Unit	Description
$\mu_{\max}^{\mathrm{diat}}$	3.5	day^{-1}	Max. phytoplankton growth rate at 0 °C
$\mu_{\max}^{\mathrm{nano}}$	3.0	day^{-1}	Max. phytoplankton growth rate at 0 °C
T_{ref}	288.15	°K	Temperature dependence factor
α^{diat}	0.19	$\mathrm{mmol\,C\,(mg\,Chl)^{-1}\,(W\,m^{-2}\,day)^{-1}}$	Initial slope of P-I curve
α^{nano}	0.14	$\mathrm{mmol\,C\,(mg\,Chl)^{-1}\,(W\,m^{-2}\,day)^{-1}}$	Initial slope of P-I curve
$K_{\mathrm{Fe}}^{\mathrm{diat}}$	0.12	$\mathrm{\mu mol\,Fe\,m^{-3}}$	Fe Half saturation coefficient
$K_{\mathrm{Fe}}^{\mathrm{nano}}$	0.02	$\mathrm{\mu mol\,Fe\,m^{-3}}$	Fe Half saturation coefficient
$\theta_{\mathrm{N/C,min}}$	0.04	$\mathrm{mol\,N\,(mol\,C)^{-1}}$	Minimum N : C ratio
$\theta_{\mathrm{Si/C,min}}$	0.04	$\mathrm{mol\,Si\,(mol\,C)^{-1}}$	Minimum Si : C ratio
$\theta_{\mathrm{min}}^{N}$	50		regulation slope
$\theta_{\mathrm{min}}^{\mathrm{Si}}$	1000		regulation slope
K_{Zoo}	0.35	$\mathrm{(mmol\,N\,m^{-3})^2}$	half-saturation constant for grazing
$u_{\max}$	2.4	day^{-1}	max. micro zoo. growth rate on nanos
Ψ_{diat}	0.5		preference coefficient for grazing on diatoms

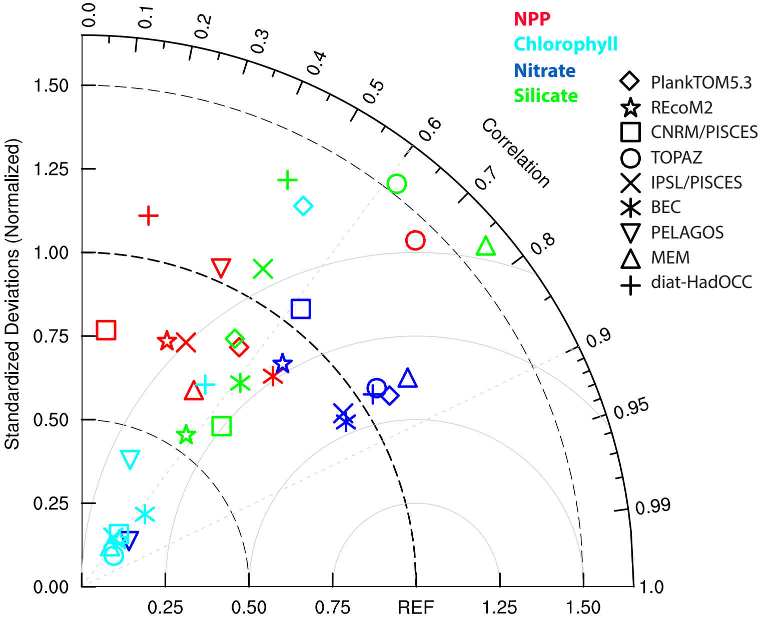

Figure 1. Taylor diagram showing the model-data correspondence for NPP (red), surface chlorophyll (light blue), NO_3 (dark blue) and SiO_3 (green). The data-based estimates are from WOA2013 for NO_3 and SiO_3, from the SeaWiFS Project for chlorophyll and from Westberry et al. (2008) for NPP. We compare nutrients for the 1990–1999 period while chlorophyll and NPP data are from 1997–2006. The angular coordinate shows the correlation coefficient, the distance from the origin denotes the normalized SD and the distance from point [1,1] describes the root mean squared error.

Title Page
Abstract
Introduction
Conclusions
References
Tables
Figures
◀|
|▶
◀
▶
Back
Close
Full Screen / Esc
Printer-friendly Version
Interactive Discussion

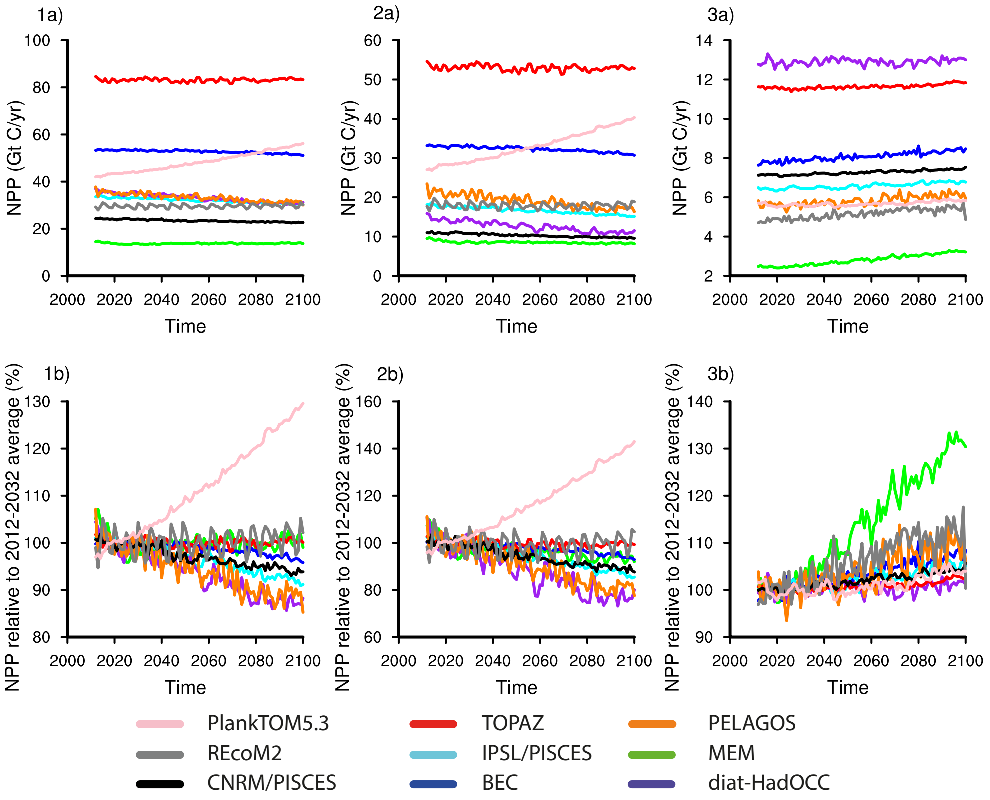

Figure 2. Projected trends in annual mean integrated net primary production (NPP) for the 2012–2100 period under RCP8.5, shown both in Gt C yr^{-1} **(a)** and in percent **(b)**. **(1a, b)** show global values, (**2a**, **b** and **3a**, **b**) show low latitudes (30° S–30° N) and Southern Ocean (90–50° S), respectively.

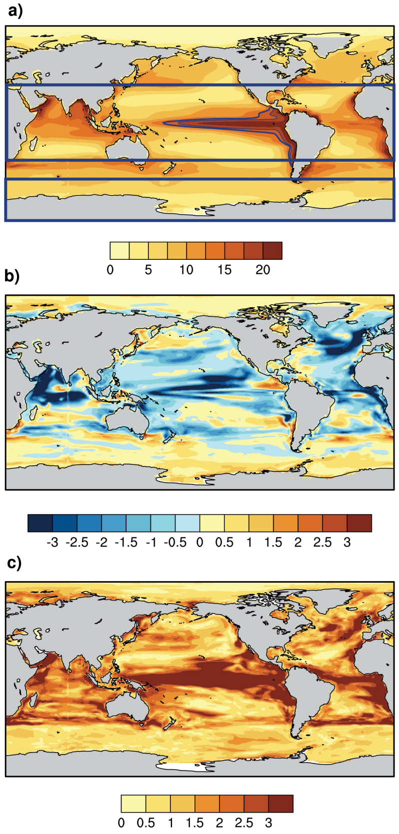

Figure 3. Spatial patterns of multi-model annual mean integrated net primary production (NPP) for **(a)** the 2012–2031 average, **(b)** changes between 2081–2100 and 2012–2031 under RCP8.5 and **(c)** interquartile range of the changes in NPP projections. The unit is mol C m^{-2} yr^{-1}. The blue boxes in **(a)** mark the regions which are discussed in more detail in this work, namely the Southern Ocean south of 50° S, the low latitudes (30° S–30° N) and the equatorial upwelling region in the Pacific.

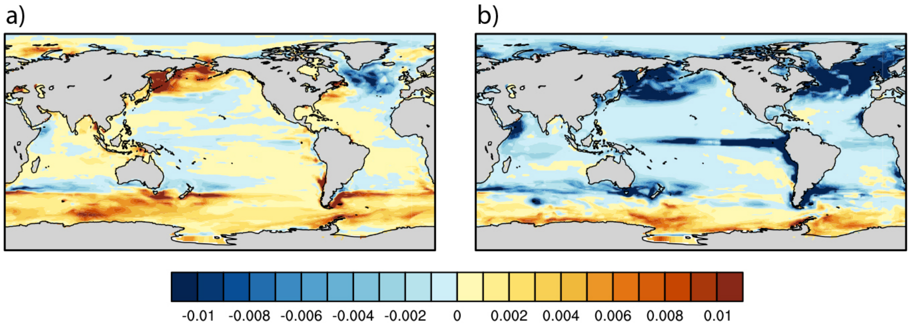

Figure 4. First order Taylor decomposition of the surface NPP changes in **(a)** biomass-weighted changes in growth and **(b)** growth-weighted changes in biomass. The unit is mol C m^{-3} yr^{-1}.

Title Page
Abstract | Introduction
Conclusions | References
Tables | Figures
◀| |▶
◀ ▶
Back | Close
Full Screen / Esc
Printer-friendly Version
Interactive Discussion

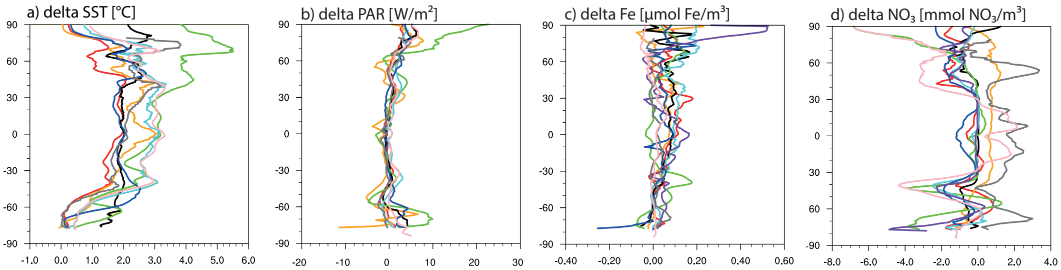

Figure 5. Zonal mean of projected sea surface temperature change, photosynthetically active radiation (PAR) change and change in surface Fe and NO$_3$ concentrations. We calculate the change as the difference between the 2012–2031 average and the 2081–2100 average. Different line colors denote different models as in the legend of Fig. 2.

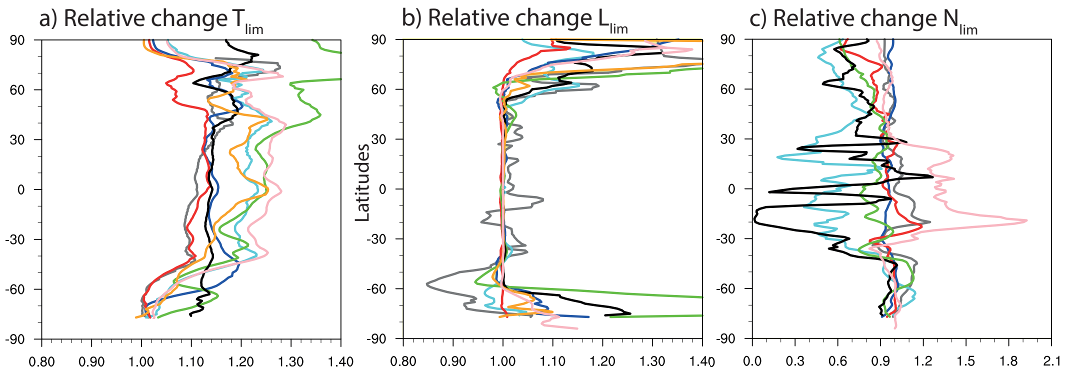

Figure 6. Zonal mean of the relative change in temperature, nutrient and light limitation. We calculate the relative change as $\frac{\text{2081–2100 average}}{\text{2012–2031 average}}$. Different line colors denote different models as in the legend of Fig. 2.

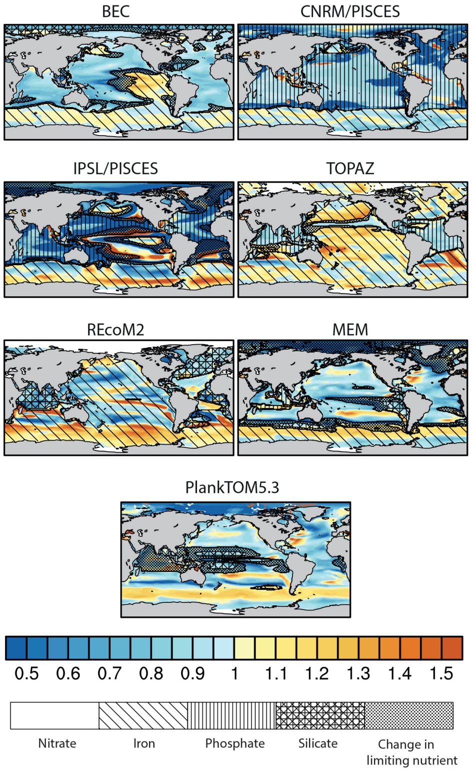

Figure 7. Changes in relative diatom nutrient limitation (calculated as the 2081–2100 average divided by the 2012–2031 average) in all models that use Liebig limitation (smallest individual nutrient limitation term determines total nutrient limitation). The colors indicate changes in the nutrient limitation value, with positive values indicating an increase in nutrient limitation factor which is equivalent to lower nutrient limitation and an increase in growth. The hatching indicates the limiting nutrient. A change in limiting nutrient during the simulation period is shown with dots. REcoM2 does not simulate the Arctic, these missing values are shown in white.

Title Page
Abstract
Introduction
Conclusions
References
Tables
Figures
◀
▶
Back
Close
Full Screen / Esc
Printer-friendly Version
Interactive Discussion

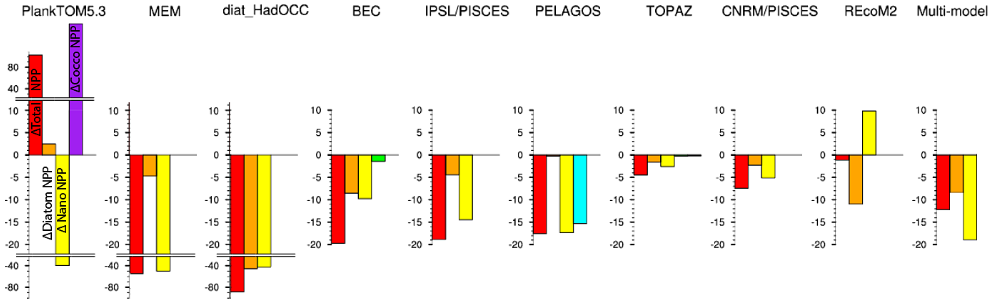

Figure 8. Decomposition of annual mean area-averaged low latitude surface NPP changes (red bar, in mol C m^{-2} yr^{-1}) into change in nanophytoplankton (yellow) and diatom (orange) surface NPP. Changes in diazotrophs (green) and picophytoplankton (light blue) have been included in the bar indicating nanophytoplankton changes for the models that simulate these functional types. For TOPAZ, changes in large non-diatom phytoplankton (dark blue) are included in the bar indicating diatom changes. Changes in coccolithophore NPP are shown in purple. Note the change in scale between the first three plots (models with large surface NPP changes) and the remaining 6 plots. While for diat-HadOCC, BEC, IPSL/PISCES, CNRM/PISCES, REcoM2 and TOPAZ the surface NPP of the PFTs was included in the model output, we show recalculated values for PlankTOM5.3, MEM and PELAGOS.

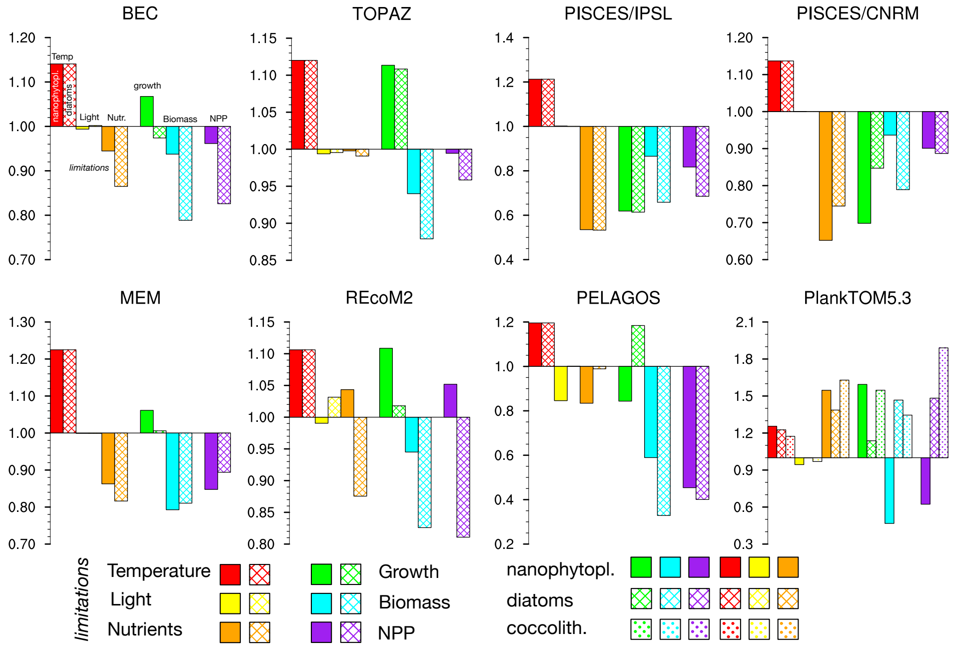

Figure 9. Relative change in temperature limitation factor (red), light limitation factor (yellow), nutrient limitation factor (orange), growth rate (green), biomass (light blue) and NPP (purple) for nanophytoplankton (full), diatoms (hatched) and coccolithophores (dotted) in the surface of the low latitudes, for all models where the full equations were available. An increase in limitation factor denotes weaker limitation, which leads to stronger growth. The relative change of a variable is the ratio between the 2081–2100 average and the 2012–2031 average. A value of one means no change, 1.2 corresponds to a 20 % increase, 0.8 corresponds to a 20 % decrease. The product of the relative change in temperature, light and nutrient limitation results approximately in the relative change in growth rate. See main text for further details.

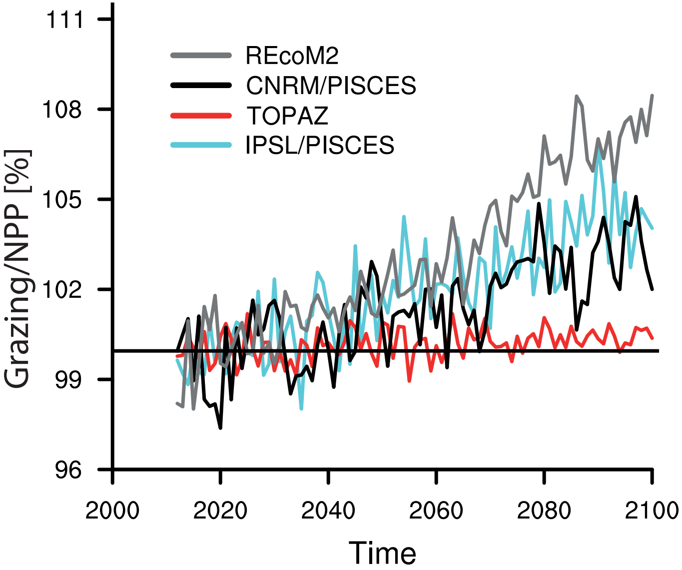

Figure 10. Fraction of NPP that is grazed (Grazing/NPP) normalized to the 2012–2031 average in the surface of the low latitudes. This plot shows data from all models where total grazing on phytoplankton is available in the output.

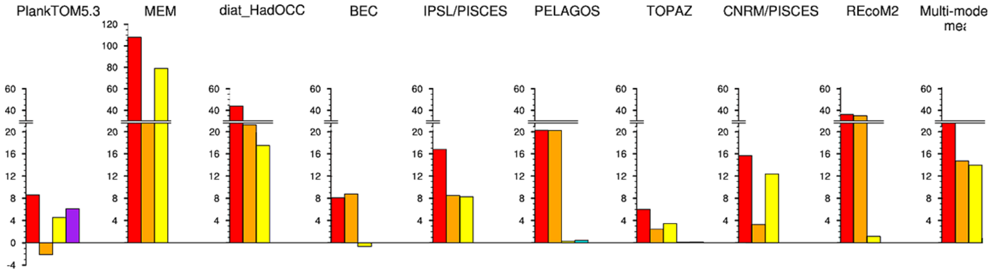

Figure 11. Decomposition of Southern Ocean (50–90° S) surface NPP trends (red bar, in $\mathrm{mol\,C\,m^{-2}\,yr^{-1}}$) into change in nanophytoplankton (yellow) and diatom (orange) surface NPP. Changes in diazotrophs (green) and picophytoplankton (light blue) have been included in the bar indicating nanophytoplankton changes for the models that simulate these functional types. For TOPAZ, changes in large non-diatom phytoplankton (dark blue) are included in the bar indicating diatom changes. Changes in coccolithophore NPP are shown in purple. Note the change in scale between the first three plots (models with large surface NPP changes) and the remaining 6 plots. While for diat-HadOCC, BEC, IPSL/PISCES, CNRM/PISCES, ReCOM2 and TOPAZ the surface NPP of the PFTs was included in the model output, we show recalculated values for PlankTOM5.3, MEM and PELAGOS.

BGD
12, 3731–3824, 2015

Drivers of future marine primary production

C. Laufkötter et al.

Title Page
Abstract
Introduction
Conclusions
References
Tables
Figures
I◀
▶I
◀
▶
Back
Close
Full Screen / Esc
Printer-friendly Version
Interactive Discussion

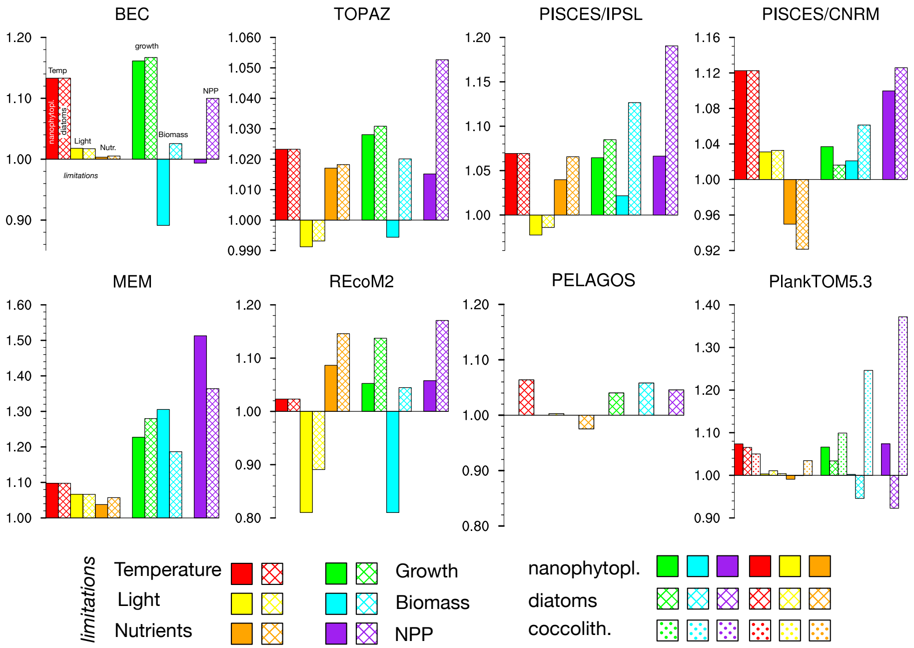

Figure 12. Relative changes in annual mean temperature limitation factor (red), light limitation factor (yellow), nutrient limitation factor (orange), growth rate (green), biomass (light blue) and NPP (purple) for nanophytoplankton (full), diatoms (hatched) and coccolithophores (dotted) in the surface of the Southern Ocean (50–90° S). An increase in limitation factor denotes weaker limitation, which leads to stronger growth. PELAGOS has a relative diatom contribution of more than 95 % of total biomass, therefore we show only results for diatoms.

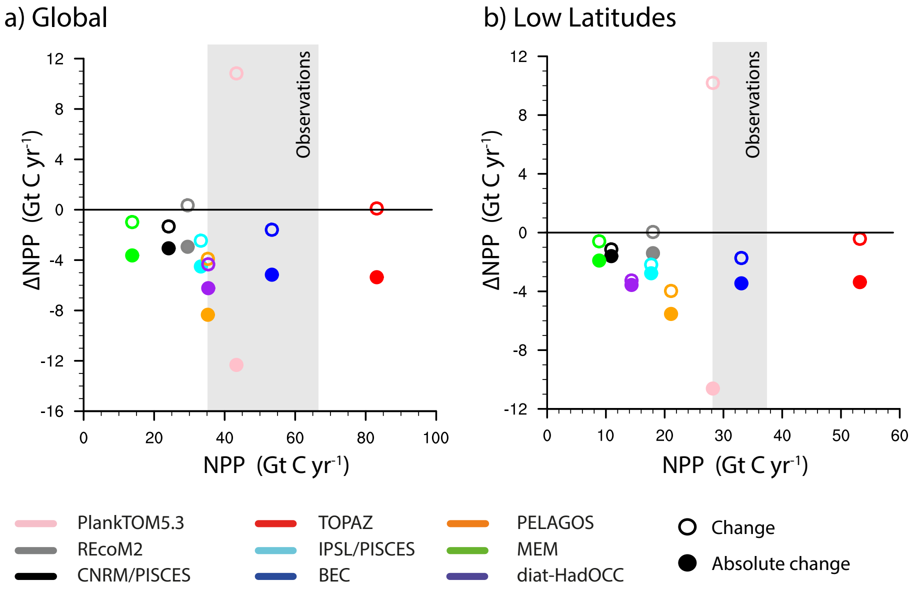

Figure 13. Relationship between the change in NPP and the 2012–2031 average NPP for all models. Change in NPP has been calculated as the sum of the differences between the 2012–2031 average and the 2081–2100 average for each grid cell (open dots). We additionally show the negative absolute differences of the changes (full dots), calculated by taking the sum of the negative absolute differences between the 2012–2031 average and the 2081–2100 average for each grid cell. Each color represents a model, **(a)** shows global values and **(b)** shows the low latitudes. The gray area marks the range of current observational NPP estimates. For global values we show the observed NPP range as reported by Carr et al. (2006), for the low latitudes we give the observed NPP range spanned by the estimates of Behrenfeld and Falkowski (1997) and Westberry et al. (2008).